SIAM J. SCI. COMPUT.
Vol. 29, No. 2, pp. 782–810

AVERAGING TECHNIQUES FOR THE A POSTERIORI BEM ERROR CONTROL FOR A HYPERSINGULAR INTEGRAL EQUATION IN TWO DIMENSIONS*

CARSTEN CARSTENSEN† AND DIRK PRAETORIUS‡

Abstract. Averaging techniques or gradient recovery techniques are frequently employed tools for the a posteriori finite element error analysis. Their very recent mathematical justification for partial differential equations allows unstructured meshes and nonsmooth exact solutions. This paper establishes an averaging technique for the hypersingular integral equation on a one-dimensional boundary and presents numerical examples that show averaging techniques can be employed for an effective mesh-refining algorithm. For the discussed test examples, the provided estimator estimates the (in general unknown) error very accurately in the sense that the quotient *error/estimator* stays bounded with a value close to 1.

Key words. averaging techniques, ZZ error estimator, hypersingular integral equation, boundary element method, Galerkin method, a posteriori error estimate, adaptive algorithm

AMS subject classifications. 65N38, 65R20, 65N50

DOI. 10.1137/050623930

1. Introduction.

This paper is devoted to the numerical treatment of the hypersingular integral equation

$$Wu = f \quad \text{on } \Gamma \tag{1.1}$$

on the relatively open boundary piece Γ of $\partial\Omega \subseteq \mathbb{R}^2$ with the hypersingular integral operator

$$(Wu)(x) = \frac{1}{\pi}\frac{\partial}{\partial n_x}\int_\Gamma u(y)\,\frac{\partial}{\partial n_y}\log|x-y|\,ds_y. \tag{1.2}$$

Here, n_x, n_y denote the outer unit normal vectors in x and y, respectively, and ds_y denotes the surface integration on Γ with respect to the variable y. For finite element methods it has recently been shown that any averaging technique [ZZ] yields reliable error estimators [CB, AC, CFuI, CFuII, CFuIII, C2]. This paper establishes analogous results for the Galerkin boundary element method (BEM) for the hypersingular integral equation (1.1). The main idea, also employed in [HSWW], goes back at least to an Oberwolfach conference in the 1980s. The first application to integral equations provides an a posteriori error analysis for Symm's integral equation [CP]. Compared with [CP], the technical details in this paper—such as an approximation result in $H^{1/2}(\Gamma)$—are more involved; cf. Theorem 3.3 below. An overview of other types of a posteriori error estimates for the Galerkin BEM can be found in [CFa].

*Received by the editors February 7, 2005; accepted for publication (in revised form) September 15, 2006; published electronically April 17, 2007. This work was supported by DFG Research Center MATHEON "Mathematics for key technologies" in Berlin and by the Austrian Science Fund FWF under grant P15274.

http://www.siam.org/journals/sisc/29-2/62393.html

†Department of Mathematics, Humboldt-Universität zu Berlin, Unter den Linden 6, D-10099 Berlin, Germany (cc@math.hu-berlin.de).

‡Institute for Analysis and Scientific Computing, Vienna University of Technology, Wiedner Hauptstrasse 8-10, A-1040 Vienna, Austria (Dirk.Praetorius@tuwien.ac.at).

Let $\mathcal{H}$ denote the Hilbert space which allows the solution of (1.1) for a given $f \in \mathcal{H}^*$; see section 2 for the precise setting. Let $\mathcal{T}_H$ be a given triangulation of Γ with mesh-size H, and let $\mathcal{T}_h$ be obtained by uniform refinements of $\mathcal{T}_H$. We consider the discrete spaces $\mathcal{S}_0^1(\mathcal{T}_h)$ and $\mathcal{S}_0^2(\mathcal{T}_H)$ consisting of all globally continuous and $\mathcal{T}_h$-piecewise affine (resp., $\mathcal{T}_H$-piecewise quadratic) splines (with respect to the arclength) which are in $\mathcal{H}$. The corresponding Galerkin projections (with respect to the energy scalar product $\langle\!\langle \cdot\,, \cdot \rangle\!\rangle$; cf. (2.11)) are denoted with $\mathbb{G}_h$ and $\mathbb{G}_H$, respectively.

Let u denote the (in general *unknown*) exact solution and $u_h = \mathbb{G}_h u \in \mathcal{S}_0^1(\mathcal{T}_h)$ be its Galerkin approximation, and consider the error estimator

$$\eta_M := |\!|\!| u_h - \mathbb{G}_H u_h |\!|\!| = \min_{v_H \in \mathcal{S}_0^2(\mathcal{T}_H)} |\!|\!| u_h - v_H |\!|\!|, \tag{1.3}$$

where $|\!|\!| v |\!|\!| := \langle\!\langle v\,, v \rangle\!\rangle^{1/2}$ denotes the energy norm. Then, Theorem 4.2 implies that

$$C_{\mathrm{eff}}\eta_M - \text{higher-order terms} \le |\!|\!| u - u_h |\!|\!| \le C_{\mathrm{rel}}\eta_M + \text{higher-order terms}, \tag{1.4}$$

where the higher-order terms depend only on the smoothness of the exact solution u. More precisely, (1.4) holds provided that u is $\mathcal{T}_H$-piecewise in $H^{2+\varepsilon}$ for some $\varepsilon > 0$. For the lower estimate in (1.4), we call the error estimator η_M *efficient*. For the upper estimate in (1.4), we say that η_M is *reliable*.

Remark 1. In order to define spaces $H^m(\mathcal{T}_H)$ of all $\mathcal{T}_H$-piecewise H^m-functions, one has to assume further regularity of the boundary piece Γ provided that $m > 1$. For the analysis below, we restrict our discussion to polygonal boundary pieces.

In contrast to the L^2 norm on Γ, which satisfies $\|\cdot\|_{L^2(\Gamma)}^2 = \sum_{\gamma \in \mathcal{T}_H} \|\cdot\|_{L^2(\gamma)}^2$, the energy norm is nonlocal. Thus, the error estimator η_M cannot be used directly for an adaptive mesh-refinement algorithm. Let H indicate the coarse triangulation $\mathcal{T}_H$ and associated quantities v_H, $\mathbb{G}_H$ as well as the (local) mesh-size as a weight in $L^2(\Gamma)$ norms, e.g., in (1.5) below. Replacing the (best approximation) operator $\mathbb{G}_H$ in the definition of η_M by an arbitrary averaging operator $\mathcal{A}_H$ onto $\mathcal{S}_0^2(\mathcal{T}_H)$, we obtain reliable error estimators $\eta_A := |\!|\!| u_h - \mathcal{A}_H u_h |\!|\!|$. By use of an inverse estimate provided in section 3.3, one verifies that

$$\mu_A := \|H^{1/2}(u_h - \mathcal{A}_H u_h)'\|_{L^2(\Gamma)} \le C_{\mathrm{inv}}\eta_A. \tag{1.5}$$

Here and throughout the paper, $(\cdot)' = \partial/\partial s$ denotes differentiation with respect to the arclengths along edges. In particular, this provides efficient error estimators

$$\mu_M := \|H^{1/2}(u_h - \mathbb{G}_H u_h)'\|_{L^2(\Gamma)} \quad \text{and} \quad \mu_\Pi := \|H^{1/2}(u_h' - \Pi_H u_h')\|_{L^2(\Gamma)}, \tag{1.6}$$

where Π_H denotes the L^2 projection onto $\mathcal{P}^1(\mathcal{T}_H)$, i.e., the $\mathcal{T}_H$-piecewise affine functions. Moreover, there also holds $\eta_M \le C\mu_M$ with some constant $C > 0$; i.e., μ_M is also reliable. Since the L^2 norm is local, the μ-estimators can be employed for an adaptive mesh-refinement.

The paper is organized as follows: Section 2 collects the preliminaries on the functional analytic setting of the hypersingular integral equation. Section 3 provides the necessary background on finite element approximation. We prove a local inverse estimate for the $H^{1/2}(\Gamma)$ norm and recall an approximation result from [C1] which is applied to the nodal interpolation operator. Section 4 is the core of this article and proves the reliability and efficiency results for the introduced error estimators. Section 5 provides details on the numerical implementation and the new adaptive mesh-refinement strategy. Four numerical experiments in section 6 conclude the work.

The examples cover a wide range, from an example with smooth solution (covered by the theory in section 4), to two examples with weak corner singularities, up to a final example on a slit which lacks almost any regularity. Even for this case, the proposed adaptive strategy recovers the optimal experimental convergence rate (in terms of number of elements).

2. Preliminaries on the functional analytic setting.

2.1. Fractional-order Sobolev spaces. Let Ω be a bounded domain in $\mathbb{R}^2$ with Lipschitz boundary $\partial\Omega$. Given $0 < \alpha \leq 1$, the Sobolev space $H^\alpha(\partial\Omega)$ is the set of all real-valued functions on $\partial\Omega$ which are the traces of functions in $H^{\alpha+1/2}(\mathbb{R}^2)$ to $\partial\Omega$,

$$H^\alpha(\partial\Omega) := \{u|_{\partial\Omega} \,:\, u \in H^{\alpha+1/2}(\mathbb{R}^2)\}. \tag{2.1}$$

Moreover, it is consistent to define $H^0(\partial\Omega) := L^2(\partial\Omega)$ and to define Sobolev spaces of negative order by duality:

$$H^{-\alpha}(\partial\Omega) := H^\alpha(\partial\Omega)^* := \text{ dual of } H^\alpha(\partial\Omega), \tag{2.2}$$

with corresponding norms and duality brackets $\langle\cdot\,,\cdot\rangle$ which extend the $L^2(\partial\Omega)$ scalar product. For the hypersingular integral equation on $\partial\Omega$, one considers the subspaces $H^\alpha_0(\partial\Omega)$ to factor the constant functions out:

$$H^\alpha_0(\partial\Omega) := H^\alpha(\partial\Omega)/\mathbb{R} = \{u \in H^\alpha(\partial\Omega) \,:\, \langle 1\,, u\rangle = 0\}, \tag{2.3}$$

where 1 denotes the constant function. For a (relatively) open subset $\omega \subseteq \Gamma$ and $\alpha \geq 0$, we define the fractional-order Sobolev space $H^\alpha(\omega)$ by extension:

$$H^\alpha(\omega) := \{u|_\omega \,:\, u \in H^\alpha(\partial\Omega)\}, \tag{2.4}$$

where the norm of $u \in H^\alpha(\omega)$ is defined as the minimal norm of an extension, i.e.,

$$\|u\|_{H^\alpha(\omega)} := \inf\{\|\widehat{u}\|_{H^\alpha(\partial\Omega)} \,:\, \widehat{u} \in H^\alpha(\partial\Omega) \text{ with } \widehat{u}|_\omega = u\}. \tag{2.5}$$

Furthermore, there are Sobolev spaces $\widetilde{H}^\alpha(\omega)$,

$$\widetilde{H}^\alpha(\omega) := \{u \in H^\alpha(\partial\Omega) \,:\, \operatorname{supp}(u) \subseteq \overline{\omega}\}, \tag{2.6}$$

associated with the usual $H^\alpha(\omega)$ norm. The corresponding spaces of negative order are again defined by duality:

$$H^{-\alpha}(\omega) = \widetilde{H}^\alpha(\omega)^* \quad \text{and} \quad \widetilde{H}^{-\alpha}(\omega) = H^\alpha(\omega)^*. \tag{2.7}$$

Remark 2. Note that $\widetilde{H}^\alpha(\partial\Omega) = H^\alpha(\partial\Omega)$. For $\omega \subsetneqq \partial\Omega$, there holds only $\widetilde{H}^\alpha(\omega) \subseteq H^\alpha(\omega)$ with

$$\|u\|_{H^\alpha(\omega)} \leq \|u\|_{\widetilde{H}^\alpha(\omega)} \quad \text{for } u \in \widetilde{H}^\alpha(\omega). \tag{2.8}$$

Remark 3. Note that according to Sobolev's inequality in one dimension each function $u \in H^\alpha(\omega)$ with $\alpha > 1/2$ is continuous. Moreover, each function $u \in H^1(\omega)$ is absolutely continuous; i.e., there holds the fundamental theorem of calculus.

2.2. Hypersingular integral operator and energy norm. Let Γ be either the closed boundary $\Gamma = \partial\Omega$ or a (relatively) open boundary piece $\omega \subseteq \partial\Omega$. We recall the mapping properties of the hypersingular integral operator (1.2).

Remark 4. (a) For a closed surface $\Gamma = \partial\Omega$, the hypersingular integral operator is a bijective, linear, and bounded operator

$$W : H_0^\alpha(\partial\Omega) \to H_0^{\alpha-1}(\partial\Omega) \tag{2.9}$$

for all indices $0 \le \alpha \le 1$. It is elliptic for $\alpha = 1/2$.

(b) For an open surface $\Gamma \subsetneqq \partial\Omega$, the hypersingular integral operator is linear and bounded as operator

$$W : \widetilde{H}^\alpha(\Gamma) \to H^{\alpha-1}(\Gamma) \tag{2.10}$$

for all indices $0 \le \alpha \le 1$ and bijective provided that $0 < \alpha < 1$. For $\alpha = 1/2$, W is a bijective and elliptic operator.

To abbreviate the notation for the energy case $\alpha = 1/2$, we define the Sobolev space $\mathcal{H}$ to be either $H_0^{1/2}(\partial\Omega)$ in the case that $\Gamma = \partial\Omega$ is closed or $\widetilde{H}^{1/2}(\Gamma)$ provided that $\Gamma \subsetneqq \partial\Omega$ is an open arc. In both cases, $W : \mathcal{H} \to \mathcal{H}^*$ is bijective and elliptic, whence W induces a scalar product on $\mathcal{H}$,

$$\langle\!\langle u, v \rangle\!\rangle := \langle Wu, v\rangle \quad \text{for } u, v \in \mathcal{H}, \tag{2.11}$$

and the corresponding *energy norm*

$$|\!|\!| u |\!|\!| := \langle\!\langle u, u \rangle\!\rangle^{1/2} \tag{2.12}$$

is an equivalent norm on $\mathcal{H} = H_0^{1/2}(\partial\Omega)$ and $\mathcal{H} = \widetilde{H}^{1/2}(\Gamma)$, respectively. According to the Lax–Milgram lemma, given $f \in \mathcal{H}^*$ there is a unique solution $u := W^{-1}f$ in $\mathcal{H}$ of (1.1).

3. Preliminaries on finite element approximation. This section recalls the Galerkin discretization of (1.1) in the Hilbert space $\mathcal{H}$ and provides some estimates for the discrete ansatz functions. Throughout we adopt the notation from the previous section.

3.1. Galerkin discretization. Let $\mathcal{T} = \{\Gamma_1, \dots, \Gamma_n\}$ be a triangulation of Γ. Each element Γ_j of the triangulation $\mathcal{T}$ is supposed to be a connected (affine) boundary piece. The set of all nodes of the triangulation $\mathcal{T}$ is denoted with $\mathcal{N}$. Let $h \in L^\infty(\Gamma)$ denote the local mesh-size $h|_{\Gamma_j} := h_j := \operatorname{diam}(\Gamma_j)$. For an integer $p \ge 0$, $\mathcal{P}_p(\mathcal{T})$ denotes the space of all piecewise polynomials of total degree $\le p$ (defined on a reference element $\Gamma_{\mathrm{ref}} = [0,1]$). Furthermore, we define globally continuous splines $\mathcal{S}^p(\mathcal{T}) := \mathcal{P}_p(\mathcal{T}) \cap \mathcal{C}(\Gamma) \subseteq H^1(\Gamma) \subseteq H^\alpha(\Gamma)$. Finally, define $\mathcal{S}_0^p(\mathcal{T})$ to be either $\{v_h \in \mathcal{S}^p(\mathcal{T}) : \langle 1, v_h\rangle = 0\}$ provided that $\Gamma = \partial\Omega$ or $\{v_h \in \mathcal{S}^p(\mathcal{T}) : v_h|_{\partial\Gamma} = 0\}$ in case $\Gamma \subsetneqq \partial\Omega$. Here, $\partial\Gamma$ denotes the set of the two endpoints of Γ. The subspace $\mathcal{S}_0^p(\mathcal{T})$ satisfies $\mathcal{S}_0^p(\mathcal{T}) \subseteq \mathcal{H}$ and will be used for a Galerkin discretization.

If $\mathcal{S}$ is a finite dimensional subspace of $\mathcal{H}$, the discrete Galerkin approximation $u_h \in \mathcal{S}$ is uniquely determined by the linear system of equations

$$\langle\!\langle u_h, v_h \rangle\!\rangle = \langle f, v_h\rangle \quad \text{for all } v_h \in \mathcal{S}. \tag{3.1}$$

The Galerkin projection $\mathbb{G} : \mathcal{H} \to \mathcal{S}$, defined by $\mathbb{G}u \in \mathcal{S}$ with

$$\langle\!\langle G_u, v_h \rangle\!\rangle = \langle\!\langle u, v_h \rangle\!\rangle \quad \text{for all } v_h \in \mathcal{S}, \tag{3.2}$$

is the orthogonal projection onto $\mathcal{S}$ with respect to the energy norm.

3.2. Standard approximation estimate. Given a regular triangulation $\mathcal{T}$, real numbers $\alpha, m \in \mathbb{R}$ with $m \geq \alpha$, and an integer $p \geq 1$, define $\widehat{p} := \min\{p+1, m\} - 1/2$. Define the $\mathcal{T}$-piecewise Sobolev space

$$H^m(\mathcal{T}) := \{v \in L^2(\Gamma) : v|_{\Gamma_j} \in H^m(\Gamma_j) \text{ for all } \Gamma_j \in \mathcal{T}\}$$

with norm $\|v\|^2_{H^m(\mathcal{T})} = \sum_{j=1}^n \|v|_{\Gamma_j}\|^2_{H^m(\Gamma_j)}$. Let $\mathbb{G}$ denote the Galerkin projection onto $\mathcal{S}^p_0(\mathcal{T})$. Then, there exists some constant $C_1 > 0$ (depending only on Γ, α, m, and p) such that

$$|||v - \mathbb{G}v||| \leq C_1 h^{\widehat{p}}_{\max} \|v\|_{H^m(\mathcal{T})} \tag{3.3}$$

for all $v \in \mathcal{H} \cap H^m(\mathcal{T})$ and $h_{\max} := \max_{\Gamma_j \in \mathcal{T}} h_j$ [SaS, sections 4.1.9 and 4.1.11].

3.3. Local inverse estimate. This subsection establishes an inverse estimate in the energy norm (see Corollary 3.2), following the arguments from [GHS]. The proof uses the fact that the Sobolev spaces can be obtained from interpolation: $H^1(\Gamma)$ can equivalently be defined as the completion of the Lipschitz continuous functions $\mathrm{Lip}(\Gamma)$ with respect to the norm $\|u\|^2_{H^1(\Gamma)} = \|u\|^2_{L^2(\Gamma)} + \|u'\|^2_{L^2(\Gamma)}$. If one defines $\widetilde{H}^1(\Gamma)$ as the completion of $\{u \in \mathrm{Lip}(\Gamma) : u|_{\partial\Gamma} = 0\}$, the Sobolev spaces $H^\alpha(\Gamma)$ and $\widetilde{H}^\alpha(\Gamma)$ satisfy

$$H^\alpha(\Gamma) = [L^2(\Gamma); H^1(\Gamma)]_\alpha \quad \text{and} \quad \widetilde{H}^\alpha(\Gamma) = [L^2(\Gamma); \widetilde{H}^1(\Gamma)]_\alpha,$$

where the brackets $[\cdot]_\alpha$ denote complex interpolation with exponent $0 \leq \alpha \leq 1$ [BL, McL]. Note that interpolation leads to the same spaces $H^\alpha(\Gamma)$ and $\widetilde{H}^\alpha(\Gamma)$, respectively, but only to equivalent norms. We will use the symbol $\lesssim$ whenever an estimate holds up to a norm equivalence constant.

Remark 5. In the context of Sobolev spaces on domains $\omega \subseteq \mathbb{R}^d$, one writes $H^1_0(\omega)$ instead of $\widetilde{H}^1(\omega)$, but this would conflict with our definition of $H^1_0(\omega)$ in (2.3).

PROPOSITION 3.1. *There is a constant $C_2 > 0$ (depending only on α, p, Γ) such that*

$$\|h^{1-\alpha} v_h'\|_{L^2(\Gamma)} \leq C_2 \|v_h\|_{H^\alpha(\Gamma)} \quad \textit{for all } v_h \in \mathcal{S}^p(\mathcal{T}). \tag{3.4}$$

Sketch of proof. We first consider the case $\alpha = 0$. For an element $\Gamma_j \in \mathcal{T}$, there holds $\|v_h'\|_{L^2(\Gamma_j)} \leq C_3\, h_j^{-1} \|v_h\|_{L^2(\Gamma_j)}$ [GHS, Proposition 2.9]. The constant $C_3 > 0$ depends only on the degree p. The summation over all $\Gamma_j \in \mathcal{T}$ leads to

$$\|h v_h'\|_{L^2(\Gamma)} \leq C_3 \|v_h\|_{L^2(\Gamma)}. \tag{3.5}$$

The combination of (3.5) with the trivial estimate $\|v_h'\|_{L^2(\Gamma)} \lesssim \|v_h\|_{H^1(\Gamma)}$ allows an interpolation argument for the operator

$$T_\alpha : \big(\mathcal{S}^p(\mathcal{T}), \|\cdot\|_{H^\alpha(\Gamma)}\big) \to \big(\mathcal{P}_{p-1}(\mathcal{T}), \|h^{1-\alpha}(\cdot)\|_{L^2(\Gamma)}\big), v_h \mapsto v_h'. \tag{3.6}$$

T_0 is continuous with operator norm $\leq C_3$, and T_1 is continuous with operator norm $\lesssim 1$. In particular, T_α is well defined and continuous with operator norm $\lesssim C_3^{1-\alpha}$. Note that the interpolation space of $(L^2, \|h(\cdot)\|_{L^2(\Gamma)})$ and $(L^2, \|\cdot\|_{L^2(\Gamma)})$ for the index $0 \leq \alpha \leq 1$ is given by $(L^2, \|h^{1-\alpha}(\cdot)\|_{L^2(\Gamma)})$ [BL, section 5.4]. ∎

Remark 6. The given proof of the inverse estimate covers a wider range of problems: The same arguments hold for $d = 3$ (i.e., v_h' is replaced by the surface gradient ∇v_h) and arbitrary $1 \leq q \leq \infty$ instead of the Hilbert case $q = 2$.

For $\alpha = 1/2$, the norm equivalence on $\mathcal{H}$ and (2.8) prove the existence of local inverse estimates in the energy norm.

COROLLARY 3.2. *There is a constant $C_{\rm inv} > 0$ which depends only on Γ and p such that*

$$\|h^{1/2} v_h'\|_{L^2(\Gamma)} \le C_{\rm inv} |\!|\!| v_h |\!|\!| \quad \text{for all } v_h \in \mathcal{S}_0^p(\mathcal{T}). \qquad \square \tag{3.7}$$

Remark 7. Since we will deal later with two discrete spaces, we are going to use superindices to indicate the mesh and the polynomial degree; e.g., $C_{\rm inv}^{h,p}$ denotes the constant in the inverse estimate (3.7) for $\mathcal{S}_0^p(\mathcal{T})$, where $\mathcal{T}$ is a mesh with (local) mesh-size $h \in L^\infty(\Gamma)$.

3.4. Local first-order approximation property. In this section we prove that the (slightly modified) nodal interpolation operator I_h onto $\mathcal{S}^1(\mathcal{T})$, for sufficiently smooth functions $v \in \mathcal{H}$, has a first-order approximation property with respect to the energy norm.

THEOREM 3.3 (see [C1]). *Suppose that Ω is a bounded Lipschitz domain in $\mathbb{R}^2$ and $\Gamma = \partial\Omega$ or $\Gamma \subsetneqq \partial\Omega$. Then, there is constant $C_\alpha > 0$ depending only on α and Γ and*

$$C_4 := \begin{cases} C_\alpha & \text{if } \alpha \neq 1/2, \\ C_\alpha \, (\log(1+\kappa))^{1/2} & \text{if } \alpha = 1/2 \end{cases} \tag{3.8}$$

for the local mesh-ratio

$$\kappa := \max\{h_j/h_k \,:\, \Gamma_j \text{ is a neighbor of } \Gamma_k\}, \tag{3.9}$$

such that there holds the localized estimate

$$\|v\|_{H^\alpha(\Gamma)} \le C_4 \, \|h^{1-\alpha} v'\|_{L^2(\Gamma)} \tag{3.10}$$

for each $v \in H^1(\Gamma)$ with at least one zero on all elements in $\mathcal{T}$. $\square$

For each node $z \in \mathcal{N}$, let $\phi_z \in \mathcal{S}^1(\mathcal{T})$ be the nodal basis function, i.e., $\mathcal{T}$-piecewise affine (with respect to the arclength) and globally continuous with $\phi_z(z) = 1$ and $\phi_z(z') = 0$ for $z' \in \mathcal{N}\backslash\{z\}$. Then, the *nodal interpolation operator* $\widehat{I}_h : \mathcal{C}(\Gamma) \to \mathcal{S}^1(\mathcal{T})$ is defined by

$$\widehat{I}_h v := \sum_{z \in \mathcal{N}} v(z) \phi_z. \tag{3.11}$$

In particular, $\widehat{I}_h v$ is well defined for any $v \in H^\alpha(\Gamma)$ and $\alpha > 1/2$. From this, we may define

$$I_h : \mathcal{C}(\Gamma) \to \mathcal{S}_0^1(\mathcal{T}), \quad I_h v := \begin{cases} \widehat{I}_h v & \text{for } \Gamma \subsetneqq \partial\Omega, \\ \widehat{I}_h v - |\Gamma|^{-1} \int_\Gamma \widehat{I}_h v \, ds & \text{for } \Gamma = \partial\Omega. \end{cases} \tag{3.12}$$

COROLLARY 3.4. *For any function $v \in H_0^1(\Gamma)$ in the case $\Gamma = \partial\Omega$ (resp., $v \in \widetilde{H}^1(\Gamma)$ in the case $\Gamma \subsetneqq \partial\Omega$), there holds with some constant $C_{\rm apx} \lesssim C_4$ (with C_4 from (3.8))*

$$|\!|\!| v - I_h v |\!|\!| \le C_{\rm apx} \|h^{1/2}(v - I_h v)'\|_{L^2(\Gamma)} \le C_{\rm apx} \|h^{1/2} v'\|_{L^2(\Gamma)}. \tag{3.13}$$

Proof for $\Gamma \subsetneqq \partial\Omega$. Since $w := v - I_h v$ has a zero on each element, namely $w(z) = 0$ for all nodes $z \in \mathcal{N}$, we may apply Theorem 3.3 together with the continuity of $W : H^{1/2}(\Gamma) \to H^{-1/2}(\Gamma)$ to obtain

$$|||w||| \le C\|w\|_{H^{1/2}(\Gamma)} \le CC_4\|h^{1/2}w'\|_{L^2(\Gamma)}.$$

The second inequality is proved elementwise: Note that there holds $\int_{\Gamma_j} w'\,ds = 0$. Therefore, $(I_h v)' \in \mathcal{P}_0(\mathcal{T})$ satisfies $(I_h v)'|_{\Gamma_j} = (1/h_j)\int_{\Gamma_j} v'\,ds$. The elementwise L^2-orthogonality shows that

$$\|w'\|^2_{L^2(\Gamma_j)} = \|v'\|^2_{L^2(\Gamma_j)} - \|(I_h v)'\|^2_{L^2(\Gamma_j)} \le \|v'\|^2_{L^2(\Gamma_j)}.$$

A summation of these estimates over $\mathcal{T}_H$ concludes the proof:

$$\|h^{1/2}w'\|^2_{L^2(\Gamma)} = \sum_{j=1}^n h_j\|w'\|^2_{L^2(\Gamma_j)} \le \sum_{j=1}^n h_j\|v'\|^2_{L^2(\Gamma_j)} = \|h^{1/2}v'\|^2_{L^2(\Gamma)}. \qquad \square$$

Proof for $\Gamma = \partial\Omega$. We define $w := v - I_h v \in H^1_0(\Gamma)$ and $\widehat{w} := w + (1/|\Gamma|)\int_\Gamma w\,ds$. Since $W1 = 0$ for the constant function 1, we have $|||w||| = |||\widehat{w}|||$. Because of $\int_\Gamma v\,ds = 0$, there holds $\widehat{w} = v - \widehat{I}_h v$. With $\widehat{w}' = w'$, we may thus apply the same arguments as in the case $\Gamma \subsetneqq \partial\Omega$ to prove (3.13). $\square$

COROLLARY 3.5. *Let $\mathcal{S}$ be a finite dimensional subspace of $H^1_0(\Gamma)$ for $\Gamma = \partial\Omega$ and of $\widetilde{H}^1(\Gamma)$ for $\Gamma \subsetneqq \partial\Omega$, respectively. Provided that $\mathcal{S}^1_0(\mathcal{T}) \subseteq \mathcal{S}$, the Galerkin projection $\mathbb{G}_h$ onto $\mathcal{S}$ satisfies*

$$|||v - \mathbb{G}_h v||| \le C_{\rm apx} \min\big\{\|h^{1/2}(v - \mathbb{G}_h v)'\|_{L^2(\Gamma)}, \|h^{1/2}v'\|_{L^2(\Gamma)}\big\} \tag{3.14}$$

for all $v \in H^1_0(\Gamma)$ (resp., $v \in \widetilde{H}^1(\Gamma)$) with the constant $C_{\rm apx} > 0$ from Corollary 3.4.

Proof. According to the best approximation property of $\mathbb{G}_h$ and Corollary 3.4, there holds

$$|||v - \mathbb{G}_h v||| \le |||v - I_h v||| \le C_{\rm apx}\|h^{1/2}v'\|_{L^2(\Gamma)}. \tag{3.15}$$

Then $w := v - \mathbb{G}_h v$ satisfies $v - \mathbb{G}_h v = w - \mathbb{G}_h w$ from the idempotency of the projection $\mathbb{G}_h$. The application of (3.15) with v replaced by w yields $|||v - \mathbb{G}_h v||| \le C_{\rm apx}\|h^{1/2}w'\|_{L^2(\Gamma)}$. $\square$

4. A posteriori error control by averaging techniques. This section aims to provide a new class of error estimators for the hypersingular integral equation and states their reliability and efficiency.

4.1. Assumptions and notation. Let $\mathcal{T}_h = \{\Gamma_1, \dots, \Gamma_n\}$ and $\mathcal{T}_H = \{\gamma_1, \dots, \gamma_N\}$ be triangulations of Γ with (local) mesh-sizes h and H, respectively, and let $\mathcal{S}_h := \mathcal{S}^1_0(\mathcal{T}_h)$ and $\mathcal{S}_H := \mathcal{S}^2_0(\mathcal{T}_H)$ be defined in section 3.1. As in Corollary 3.4, let $I_h : H^1(\Gamma) \to \mathcal{S}_h$ denote the nodal interpolation operator onto $\mathcal{S}_h$ with approximation constant $C_{\rm apx} > 0$, and let $C^{H,2}_{\rm inv} > 0$ denote the constant in the inverse estimate (3.7) for $\mathcal{S}_H$. We assume that the mesh-size h is small enough when compared to H; more precisely,

$$C_{\rm apx}C^{H,2}_{\rm inv} \max_{\gamma_j \in \mathcal{T}_H} (\|h\|_{L^\infty(\gamma_j)}/H_j)^{1/2} =: L < 1. \tag{4.1}$$

Moreover, the analysis in the subsequent sections requires an additional regularity assumption on the exact solution $u \in \mathcal{H}$ of (1.1), namely,

$$u \in H^m(\mathcal{T}_H) \quad \text{for some } m > 2. \tag{4.2}$$

4.2. General results. Let $u \in \mathcal{H}$ denote the unique solution of (1.1), and let $u_h \in \mathcal{S}_h$ be its Galerkin approximation with respect to $\mathcal{S} = \mathcal{S}_h$ in (3.1). The Galerkin projection $\mathbb{G}_H$ onto $\mathcal{S}_H$ (i.e., the orthogonal projection onto $\mathcal{S}_H$ with respect to the energy norm) is compared with an *arbitrary* (not necessarily linear or continuous) operator

$$\mathcal{A}_H : L^2(\Gamma) \to \mathcal{S}_H. \tag{4.3}$$

The main results of this section are stated in Theorem 4.2 and Corollaries 4.3–4.5.

PROPOSITION 4.1. *Under assumption* (4.1)*, there holds*

$$|||u - u_h||| \le |||(\mathbb{1} - \mathbb{G}_H)(u - u_h)|||/(1 - L). \tag{4.4}$$

Proof. Define $\widetilde{h} \in \mathcal{P}_0(\mathcal{T}_H)$ by $\widetilde{h}|_{\gamma_j} := \|h\|_{L^\infty(\gamma_j)}$ for each element $\gamma_j \in \mathcal{T}_H$. For the Galerkin error $e := u - u_h$, the approximation property (3.13) of I_h yields

$$|||(\mathbb{1} - I_h)\mathbb{G}_H e||| \le C_{\rm apx}\|h^{1/2}(\mathbb{G}_H e)'\|_{L^2(\Gamma)} \le C_{\rm apx}\|\widetilde{h}^{1/2}(\mathbb{G}_H e)'\|_{L^2(\Gamma)}.$$

Now, we use the inverse estimate (3.7) for $\mathbb{G}_H e \in \mathcal{S}_H$ and infer that

$$\begin{aligned}\|\widetilde{h}^{1/2}(\mathbb{G}_H e)'\|_{L^2(\Gamma)} &\le \|(\widetilde{h}/H)^{1/2}\|_{L^\infty(\Gamma)}\|H^{1/2}(\mathbb{G}_H e)'\|_{L^2(\Gamma)}\\ &\le C_{\rm inv}^{H,2}\|(\widetilde{h}/H)^{1/2}\|_{L^\infty(\Gamma)}|||\mathbb{G}_H e|||.\end{aligned}$$

The combination with the best approximation property $|||\mathbb{G}_H e||| \le |||e|||$ shows that

$$|||(\mathbb{1} - I_h)\mathbb{G}_H e||| \le L|||e|||.$$

Using the Galerkin orthogonality and a Cauchy inequality, we obtain for $I_h\mathbb{G}_H e \in \mathcal{S}_h$

$$\langle\!\langle e, \mathbb{G}_H e\rangle\!\rangle = \langle\!\langle e, \mathbb{G}_H e - I_h\mathbb{G}_H e\rangle\!\rangle \le |||e|||\,|||(\mathbb{1} - I_h)\mathbb{G}_H e||| \le L|||e|||^2.$$

A further application of the Cauchy inequality concludes the proof:

$$|||e|||^2 = \langle\!\langle e, \mathbb{G}_H e\rangle\!\rangle + \langle\!\langle e, e - \mathbb{G}_H e\rangle\!\rangle \le |||e|||\,\big(L|||e||| + |||(\mathbb{1} - \mathbb{G}_H)e|||\big). \qquad \square$$

THEOREM 4.2. *Assume* (4.1)–(4.2)*. Then the error estimator*

$$\eta_M := |||u_h - \mathbb{G}_H u_h|||$$

is reliable in the sense of

$$|||u - u_h||| \le \big(\eta_M + |||(\mathbb{1} - \mathbb{G}_H)u|||\big)/\big(1 - L\big) \tag{4.5}$$

and efficient in the sense of

$$\eta_M \le |||u - u_h||| + |||(\mathbb{1} - \mathbb{G}_H)u|||. \tag{4.6}$$

(Compared with $|||u - u_h|||$ and η_M, the term $|||(\mathbb{1} - \mathbb{G}_H)u|||$ is generically of higher order.)

Proof. According to (3.3), the error in the energy norm is of order

$$|||u - u_h||| = O(h_{\rm max}^{\widehat{p}}) \quad \text{with} \quad \widehat{p} := \min\{2, m\} - 1/2 = 3/2.$$

Furthermore, for smooth u we have

$$|||(\mathbb{1}-\mathbb{G}_H)u||| = O(H_{\max}^{\widehat{q}}) \quad \text{with } \widehat{q} := \min\{3,m\} - 1/2 > 3/2.$$

Since $m > 2$, $|||(\mathbb{1}-\mathbb{G}_H)u|||$ is of higher order. The combination of Proposition 4.1 with a triangle inequality shows that

$$|||u-u_h||| \le \big(|||(\mathbb{1}-\mathbb{G}_H)u||| + |||(\mathbb{1}-\mathbb{G}_H)u_h|||\big)/\big(1-L\big).$$

This proves reliability. A simple triangle inequality,

$$\eta_M \le |||(\mathbb{1}-\mathbb{G}_H)(u-u_h)||| + |||(\mathbb{1}-\mathbb{G}_H)u||| \le |||u-u_h||| + |||(\mathbb{1}-\mathbb{G}_H)u|||,$$

shows efficiency since $(\mathbb{1}-\mathbb{G}_H)$ is an orthogonal projection with respect to the energy norm. ∎

Replacing the best approximation operator $\mathbb{G}_H$ by the operator $\mathcal{A}_H$, we immediately obtain the following corollary.

COROLLARY 4.3. *We always have $\eta_M \le \eta_A := |||u_h - \mathcal{A}_H u_h|||$; i.e., under the assumptions* (4.1)–(4.2) *the error estimator η_A is reliable.* ∎

To develop an adaptive mesh-refining algorithm, we have to provide an error estimator which can be localized. More precisely, we will estimate the nonlocal $\mathcal{H}$ norm by the (weighted) local H^1 seminorm, namely $\mu_M := \|H^{1/2}(u_h - \mathbb{G}_H u_h)'\|_{L^2(\Gamma)}$.

COROLLARY 4.4. *As $\mathcal{S}^1_0(\mathcal{T}_H) \subseteq \mathcal{S}_H$, there holds with the constant $C_{\rm apx} > 0$ from Corollary* 3.4

$$\eta_M \le C_{\rm apx}\mu_M. \tag{4.7}$$

Therefore, μ_M is reliable under assumptions (4.1)–(4.2).

Proof. The proof follows immediately from the approximation property of the Galerkin projection (3.14). ∎

COROLLARY 4.5. *Suppose that $\mathcal{S}_H \subseteq \mathcal{S}^2(\mathcal{T}_h)$. Then, there holds*

$$\mu_A := \|H^{1/2}(u_h - \mathcal{A}_H u_h)'\|_{L^2(\Gamma)} \le C_5 C_{\rm inv}^{h,2}\eta_A \tag{4.8}$$

with the constant $C_5 := \max\{\|H\|_{L^\infty(\Gamma_j)}/h_j : \Gamma_j \in \mathcal{T}\}$ and the constant $C_{\rm inv}^{h,2} > 0$ for an inverse estimate on $\mathcal{S}^2(\mathcal{T}_h)$. With Π_H denoting the L^2 projection onto $\mathcal{P}^1(\mathcal{T}_H)$, the error estimators μ_M and $\mu_\Pi := \|H^{1/2}(u_h' - \Pi_H u_h')\|_{L^2(\Gamma)}$ satisfy

$$\mu_\Pi \le \mu_M \le C_5 C_{\rm inv}^{h,2}\eta_M \tag{4.9}$$

and therefore are efficient under assumptions (4.1)–(4.2).

Proof. The estimate (4.8) follows from the inverse estimate (3.7), and so does the second estimate in (4.9). Note that Π_H is the *elementwise* L^2 projection. This proves $\|u_h' - \Pi_H u_h'\|_{L^2(\gamma_j)} \le \|u_h' - (\mathbb{G}_H u_h)'\|_{L^2(\gamma_j)}$ for any $\gamma_j \in \mathcal{T}_H$. Summing the H-weighted L^2 norms over all elements $\gamma_j \in \mathcal{T}_H$, we prove (4.9). ∎

Remark 8. Note that the assumption $\mathcal{S}_H = \mathcal{S}^2_0(\mathcal{T}_H) \subseteq \mathcal{S}^2(\mathcal{T}_h)$ is quite weak and satisfied if $\mathcal{T}_h$ is obtained from $\mathcal{T}_H$ by some (local) refinements.

4.3. Reliability of μ_A for the L^2 projection. As proved in Corollary 4.5, there holds $\mu_A \le C_5 C_{\rm inv}^{h,2}\,\eta_A$ under weak assumptions on $\mathcal{T}_H$. To obtain the converse estimate $\eta_A \le C_6\,\mu_A$ with a constant C_6 which depends on neither the mesh-sizes nor the number of elements, one has to prove

$$|||v_h - \mathcal{A}_H v_h||| \le C_6\|H^{1/2}(v_h - \mathcal{A}_H v_h)'\|_{L^2(\Gamma)} \quad \text{for all } v_h \in \mathcal{S}_h. \tag{4.10}$$

One then obtains the equivalence of the error estimators μ_A and η_A and, in particular, the reliability of μ_A under the assumptions (4.1)–(4.2). This is done for the L^2 projection $\mathcal{A}_H$ onto $\mathcal{S}_H$ in the following proposition.

PROPOSITION 4.6. *Let $\mathcal{A}_H$ be the L^2-orthogonal projection onto $\mathcal{S}_H$. Under the assumptions of Corollary* 4.5, *the error estimator μ_A from* (4.8) *satisfies*

$$C_6^{-1}\eta_A \le \mu_A \le C_5 C_{\mathrm{inv}}^{h,2}\,\eta_A. \tag{4.11}$$

Proof for $\Gamma = \partial\Omega$. Since the L^2 projection $\mathbb{P}_H : H_0^1(\Gamma) \to \mathcal{S}^2(\mathcal{T}_H)$ satisfies

$$0 = \langle 1\,, (\mathbb{1} - \mathbb{P}_H)u_h\rangle = \langle 1\,, u_h\rangle - \langle 1\,, \mathbb{P}_H u_h\rangle = -\langle 1\,, \mathbb{P}_H u_h\rangle,$$

there holds $\mathbb{P}_H u_h \in \mathcal{S}_H$. Consequently, $\mathbb{P}_H u_h = \mathcal{A}_H u_h$ and $(\mathbb{1} - \mathcal{A}_H)u_h$ is L^2-orthogonal to $\mathcal{S}^2(\mathcal{T}_H)$. Let $\gamma_j \in \mathcal{T}_H$ be a coarse grid element with nodes $z, z' \in \mathcal{N}_H$. We define the bubble function $\beta_j(x) := \phi_{H,z}(x)\phi_{H,z'}(x)$ for $x \in \Gamma$ as the product of the corresponding hat functions. Then, $\beta_j \in \mathcal{S}^2(\mathcal{T}_H)$ is positive on the interior γ_j. With $v := (\mathbb{1} - \mathcal{A}_H)u_h$ there holds

$$0 = \langle \beta_j\,, v\rangle = \int_{\gamma_j} \beta_j v\, ds. \tag{4.12}$$

Therefore, v has at least one zero in γ_j so that Theorem 3.3 can be applied for $\mathcal{T}_H$. ∎

Proof for $\Gamma \subsetneqq \partial\Omega$. The bubble functions vanish in all nodes $z \in \mathcal{N}_H$ and hence satisfy $\beta_j \in \mathcal{S}_H$ for all $1 \le j \le n$. Therefore, (4.12) holds and we can apply Theorem 3.3 again. ∎

Remark 9. The approximation argument in the proof of Proposition 4.6 works for sufficiently smooth $\widetilde{u} \in \mathcal{H}$ instead of $u_h \in \mathcal{S}_h$; e.g., u_h may be replaced by some $\widetilde{u}$ in $H_0^1(\Gamma)$ (resp., $\widetilde{H}^1(\Gamma)$).

In the case that $\Gamma \subsetneqq \partial\Omega$ is an open boundary piece, it is easy to construct operators which satisfy (4.10) since we only have to satisfy the zero boundary conditions for discrete functions at the endpoints of Γ.

Remark 10. Suppose that $\Gamma \subsetneqq \partial\Omega$. Let $\mathcal{A}_H$ be the pointwise interpolation operator satisfying

$$\mathcal{A}_H u_h \in \mathcal{S}^2(\mathcal{T}_H) \quad \text{and} \quad \mathcal{A}_H u_h(z) = u_h(z) \quad \text{for } z \in \{a_j, m_j, b_j\},$$

where a_j and b_j denote the nodes of γ_j and m_j denotes the element's midpoint. Note that $\mathcal{A}_H u_h$ vanishes at the endpoints of Γ. Therefore, $\mathcal{A}_H u_h \in \mathcal{S}_H$ and according to Theorem 3.3 there holds (4.10).

Remark 11. Suppose that $\mathcal{A}_H$ is idempotent; i.e., $\mathcal{A}_H^2 = \mathcal{A}_H$. Then, an elementary algebraic manipulation shows that (4.10) follows from the approximation estimate

$$|\!|\!| v_h - \mathcal{A}_H v_h |\!|\!| \le C_5 \|H^{1/2} v_h'\|_{L^2(\Gamma)}$$

for all $v_h \in \mathcal{S}_H$.

5. Numerical realization. As in the previous section, we write $\mathcal{S}_h = \mathcal{S}_0^1(\mathcal{T}_h)$ and $\mathcal{S}_H = \mathcal{S}_0^2(\mathcal{T}_H)$. The finer mesh $\mathcal{T}_h$ is obtained from the coarser $\mathcal{T}_H$ by uniform refinements; see section 5.5 for details. This ensures $\mathcal{S}_H = \mathcal{S}_0^2(\mathcal{T}_H) \subseteq \mathcal{S}^2(\mathcal{T}_h)$ as in Corollary 4.5.

5.1. Neumann problem and hypersingular integral equation. In the numerical experiments we consider examples where the right-hand side f in (1.1) comes from a Neumann problem

$$\Delta U = 0 \text{ in } \Omega \quad \text{and} \quad \partial U/\partial\nu = g \text{ on } \Gamma = \partial\Omega \tag{5.1}$$

with given Neumann data g on Γ (plus boundary conditions at infinity if Ω is unbounded) and the normal derivative $\partial U/\partial\nu$, where ν denotes the outer unit vector on $\partial\Omega$. This problem is equivalent to the hypersingular integral equation (1.1), where f takes the form

$$f = (\mathbb{1} - K^*)g \tag{5.2}$$

with the adjoint double-layer potential operator K^*, defined as Cauchy principal value by

$$(K^*g)(x) := -\frac{1}{\pi} \int\!\!\!\!\!\!- _\Gamma g(y)\, \frac{(y-x)\cdot\nu(x)}{|x-y|^2}\, ds_y \quad \text{for } x \in \Gamma. \tag{5.3}$$

Up to an additive constant, the exact solution of (1.1) is just the Dirichlet data $U|_\Gamma$ of U on the boundary Γ. More precisely, there holds $u = U|_\Gamma - \langle U|_\Gamma\,, 1\rangle/\langle 1\,, 1\rangle$.

5.2. Computation of the discrete solution for $\Gamma = \partial\Omega$. The problem to solve (1.1) in the Hilbert space $H^\alpha_0(\Gamma)$ can equivalently be formulated as follows [CoS, CaS]: Given $(f, b) \in H^{\alpha-1}(\Gamma) \times \mathbb{R}$, find $(u, a) \in H^\alpha(\Gamma) \times \mathbb{R}$ such that

$$Wu + a = f \quad \text{and} \quad \langle 1\,, u\rangle = b. \tag{5.4}$$

The corresponding discrete formulation reads as follows: Find $(u_h, a_h) \in \mathcal{S}^1(\mathcal{T}) \times \mathbb{R}$ such that

$$\langle Wu_h + a_h\,, v_h\rangle = \langle f\,, v_h\rangle \quad \text{for all } v_h \in \mathcal{S}^1(\mathcal{T}_h) \quad \text{and} \quad \langle 1\,, u_h\rangle = b. \tag{5.5}$$

Notice that $\langle 1\,, u - u_h\rangle = 0$, whence $u - u_h \in H^\alpha_0(\Gamma)$, and $\langle 1\,, f - a_h\rangle = \langle 1\,, Wu_h\rangle = 0$; i.e., $a_h = \langle f\,, 1\rangle/\langle 1\,, 1\rangle$ and $f - a_h \in H^{\alpha-1}_0(\Gamma)$. In particular, for $b = 0$ and $f \in H^{\alpha-1}_0(\Gamma)$, the solution of (5.4) (resp., (5.5)) is just the solution of (1.1) (resp., (3.1)). The benefit of the generalized formulation is that we are allowed to consider the full discrete space $\mathcal{S}^1(\mathcal{T}_h)$ instead of $\mathcal{S}^1_0(\mathcal{T}_h)$. This simplifies the implementation since one can use the usual nodal hat functions instead of a basis of $\mathcal{S}^1_0(\mathcal{T}_h)$.

Let $\mathcal{N}_h$ denote the set of all nodes of $\mathcal{T}_h$ and, with $n := |\mathcal{N}_h|$, define the (symmetric) stiffness matrix $\mathbf{A}$ by

$$\mathbf{A}_{jk} = \langle\!\langle \phi_j\,, \phi_k\rangle\!\rangle \quad \text{for } 1 \le j, k \le n, \tag{5.6}$$

with $\phi_j, \phi_k \in \mathcal{S}^1(\mathcal{T}_h)$ denoting the hat functions corresponding to the jth and kth node, and

$$\mathbf{A}_{j,n+1} = \mathbf{A}_{n+1,j} = \langle 1\,, \phi_j\rangle, \quad \mathbf{A}_{n+1,n+1} = 0. \tag{5.7}$$

With the right-hand side

$$\mathbf{b}_j = \langle f\,, \phi_j\rangle \quad \text{for } 1 \le j \le n, \tag{5.8}$$

the discrete solution u_h of (3.1) has the basis representation

$$u_h = \sum_{j=1}^{n} \mathbf{x}_j \phi_j, \tag{5.9}$$

where the coefficient vector $\mathbf{x} \in \mathbb{R}^{n+1}$ solves the linear system $\mathbf{A}\mathbf{x} = \mathbf{b}$ with $\mathbf{b}_{n+1} := 0$. Moreover, there holds $x_{n+1} = a_h$ with a_h from (5.5).

Remark 12. (a) The hypersingular integral operator (1.2) and the single-layer potential

$$(Vu)(x) := -\frac{1}{\pi} \int_\Gamma u(y) \log|x-y| \, ds_y \tag{5.10}$$

are linked through Nédélec's equation (recall $(\cdot)' = \partial/\partial s$)

$$\langle Wu \, , v \rangle = \langle Vu' \, , v' \rangle \quad \text{for all } u, v \in \mathcal{H}. \tag{5.11}$$

(b) According to (a), the entries of $\mathbf{A}$ in (5.6) can be computed analytically using (5.11) and exact integration for the single-layer potential; see [Ma].

5.3. Computation of the discrete solution for $\Gamma \subsetneqq \partial\Omega$. Let $\mathcal{K}_h := \mathcal{N}_h \backslash \partial\Gamma$ denote the set of all interior nodes of $\mathcal{T}$. Then, the implementation for an open curve is less involved since the hat functions ϕ_j with $j \in \mathcal{K}_h$ form the nodal basis of $\mathcal{S}^1_0(\mathcal{T}_h)$. With $n := |\mathcal{K}_h|$, we compute $\mathbf{A}$ and $\mathbf{b}$ as in (5.6) and (5.8), respectively. Then, the discrete solution u_h is represented as in (5.9) with $\mathbf{x} \in \mathbb{R}^n$ satisfying $\mathbf{A}\mathbf{x} = \mathbf{b}$.

Remark 13. For implementational reasons, the matrix $\mathbf{A}$ and the right-hand side $\mathbf{b}$ are computed for all hat functions, i.e., $\mathcal{N}_h$, and the resulting linear system is solved only on a subblock corresponding to $\mathcal{K}_h$.

5.4. Computation of the right-hand side for academic examples. If the exact solution $u \in \mathcal{H}$ is known, the entries for the right-hand side vector (cf. (5.8)), can easily be obtained by use of Remark 12: According to (5.11), there holds

$$\mathbf{b}_j = \langle f \, , \phi_j \rangle = \langle Wu \, , \phi_j \rangle = \langle u' \, , V\phi_j' \rangle.$$

Notice that the integrand $b(x) = u'(x)(V\phi_j')(x)$ may have logarithmic singularities. For the numerical experiments, we used the `quad` function implemented in MATLAB, which is based on an h-adaptive Simpson formula and Romberg extrapolation.

5.5. Adaptive algorithm. All mesh-refinements are performed with the following adaptive algorithm from [CP] based on the refinement indicators $\mu_{M,j}$, $\mu_{A,j}$, and $\mu_{\Pi,j}$ defined as follows: Given the coarse mesh $\mathcal{T}_H = \{\gamma_1, \dots, \gamma_N\}$ and the L^2 projections $\Pi^1_H : \mathcal{S}_h \to \mathcal{S}^1_0(\mathcal{T}_H)$ and $\Pi^2_H : \mathcal{S}_h \to \mathcal{S}^2_0(\mathcal{T}_H)$, we define, for $j = 1, \dots, N$,

$$\mu_{M,j} := H_j^{1/2} \| u_h' - (\mathbb{G}_H u_h)' \|_{L^2(\gamma_j)}, \tag{5.12}$$

$$\mu_{A,j} := H_j^{1/2} \| u_h' - (\Pi^2_H u_h)' \|_{L^2(\gamma_j)}, \tag{5.13}$$

$$\mu_{\Pi,j} := H_j^{1/2} \| u_h' - \Pi^1_H(u_h') \|_{L^2(\gamma_j)}, \tag{5.14}$$

i.e., $\mu_M = \big(\sum_{j=1}^N \mu_{M,j}^2\big)^{1/2}$, $\mu_A = \big(\sum_{j=1}^N \mu_{A,j}^2\big)^{1/2}$, and $\mu_\Pi = \big(\sum_{j=1}^N \mu_{\Pi,j}^2\big)^{1/2}$, respectively.

ALGORITHM 5.1. *Choose an initial mesh* $\mathcal{T}_H^{(0)}$, $k = 0$, $\ell \in \mathbb{N}_{\geq 2}$, *and* $0 \leq \theta \leq 1$.

(i) *Obtain* $\mathcal{T}_h^{(k)} = \{\Gamma_1, \dots, \Gamma_n\}$ *from* $\mathcal{T}_H^{(k)} = \{\gamma_1, \dots, \gamma_N\}$ *by uniform splitting of each element* $\gamma_j \in \mathcal{T}_H^{(k)}$ *into* ℓ *elements of equal length.*

(ii) *Compute the approximation* $u_h^{(k)}$ *for the current mesh* $\mathcal{T}_h^{(k)}$.

(iii) *Compute error estimators* η_M *and* η_A *and refinement indicators* $\mu_{M,j}$, $\mu_{A,j}$, *and* $\mu_{\Pi,j}$.

(iv) *Mark element* γ_j *provided the corresponding refinement estimator satisfies* $\mu_{M,j} \geq \theta \max\{\mu_{M,1}, \dots, \mu_{M,N}\}$ *(or* $\mu_{M,j}$ *replaced by* $\mu_{A,j}$ *and* $\mu_{\Pi,j}$, *respectively).*

(v) *Halve all marked elements* $\gamma_j \in \mathcal{T}_H^{(k)}$ *and so generate a new coarse mesh* $\mathcal{T}_H^{(k+1)}$, *update* k, *and go to* (i).

Remark 14. The choice of $\theta = 0$ in Algorithm 5.1 leads to uniform mesh-refinement, whereas we used $\theta = 1/2$ for adaptive mesh-refinement in the subsequent numerical examples. The parameter $\ell \in \mathbb{N}_{\geq 2}$ is chosen between 2 and 4 and is empirically discussed later.

Remark 15. Since the local mesh-ratio $\kappa(\mathcal{T}_h^{(h)})$ defined in (3.9) enters the constant $C_{\rm apx}$ and thus affects the reliability of our estimators, we mark further elements for refinement to guarantee $\kappa(\mathcal{T}_H^{(k)}) \leq 2\kappa(\mathcal{T}_H^{(0)})$. Note that there holds $\kappa(\mathcal{T}_h^{(k)}) = \kappa(\mathcal{T}_H^{(k)})$.

5.6. Computation of the error estimators. Let $\phi_1, \dots, \phi_n$ be a basis of $\mathcal{S}_h$ and $\Phi_1, \dots, \Phi_N$ be a basis of $\mathcal{S}_H$ and define the matrices $\mathbf{A} \in \mathbb{R}^{n\times n}_{sym}$, $\mathbf{B} \in \mathbb{R}^{N\times N}_{sym}$, and $\mathbf{C} \in \mathbb{R}^{N\times n}$ by

$$\mathbf{A}_{jk} := \langle\!\langle \phi_j, \phi_k \rangle\!\rangle, \quad \mathbf{B}_{jk} := \langle\!\langle \Phi_j, \Phi_k \rangle\!\rangle, \quad \text{and} \quad \mathbf{C}_{jk} := \langle\!\langle \Phi_j, \phi_k \rangle\!\rangle. \tag{5.15}$$

Let $\mathbf{x} \in \mathbb{R}^n$ be the coefficient vector of $u_h \in \mathcal{S}_h$ and $\mathbf{y} \in \mathbb{R}^N$ the coefficient vector of $\mathbb{G}_H u_h \in \mathcal{S}_H$. Note that the vector $\mathbf{y}$ is the solution of the linear system $\mathbf{By} = \mathbf{Cx}$. Then, Galerkin orthogonality yields

$$\eta_M^2 = |\!|\!| u_h - \mathbb{G}_H u_h |\!|\!|^2 = |\!|\!| u_h |\!|\!|^2 - |\!|\!| \mathbb{G}_H u_h |\!|\!|^2 = \mathbf{x} \cdot \mathbf{Ax} - \mathbf{y} \cdot \mathbf{By} = \mathbf{x} \cdot (\mathbf{Ax} - \mathbf{C}^T\mathbf{y}).$$

The computation of the error estimator η_A involves the L^2 mass matrices $\widehat{\mathbf{B}} \in \mathbb{R}^{N\times N}_{sym}$ and $\widehat{\mathbf{C}} \in \mathbb{R}^{N\times n}$ defined by

$$\widehat{\mathbf{B}}_{jk} := \langle \Phi_j, \Phi_k \rangle \quad \text{and} \quad \widehat{\mathbf{C}}_{jk} := \langle \Phi_j, \phi_k \rangle. \tag{5.16}$$

If $\mathcal{A}_H$ denotes the L^2 projection onto $\mathcal{S}_H$, the coefficient vector $\widehat{\mathbf{y}} \in \mathbb{R}^N$ of $\mathcal{A}_H u_h$ is the solution of the linear system $\widehat{\mathbf{B}}\mathbf{y} = \widehat{\mathbf{C}}\mathbf{x}$. Then, η_A reads as

$$\eta_A^2 = |\!|\!| u_h - \mathcal{A}_H u_h |\!|\!|^2 = \mathbf{x} \cdot \mathbf{Ax} - \widehat{\mathbf{y}} \cdot (2\,\mathbf{Cx} - \mathbf{B}\widehat{\mathbf{y}}).$$

Remark 16. (a) In case $\Gamma = \partial\Omega$, it is convenient to extend $\mathbf{A}$, $\mathbf{B}$, and $\widehat{\mathbf{B}}$ by a side-constraint analogously to (5.7) and then to consider a basis of $\mathcal{S}^1(\mathcal{T}_h)$ and $\mathcal{S}^2(\mathcal{T}_h)$ instead of $\mathcal{S}_h$ and $\mathcal{S}_H$, respectively.

(b) The entries of $\mathbf{A}, \mathbf{B}, \mathbf{C}$ are computed analytically by use of Remark 12 for ϕ_j being a hat function in $\mathcal{S}^1(\mathcal{T}_h)$ and Φ_j being either a hat function in $\mathcal{S}^1(\mathcal{T}_H)$ or a bubble function in $\mathcal{S}^2(\mathcal{T}_H)$, i.e., the product of two hat functions with overlapping support.

(c) The entries of $\widehat{\mathbf{B}}$ are computed analytically by transforming the arising integrals to the reference element $[0, 1]$, where the hat functions are given by t and $1 - t$ and the corresponding bubble is $t(1 - t)$.

(d) The entries of $\widehat{\mathbf{C}}$ are easily computed since a fine grid element $\Gamma_j \in \mathcal{T}_h$ lies in precisely one coarse grid element $\gamma_k \in \mathcal{T}_H$. If we use the arclength parametrization of γ_k, Γ_j then corresponds to a subinterval $[a,b] \subseteq [0, H_k]$.

(e) The error estimators μ_M and μ_A are computed $\mathcal{T}_H$-elementwise as indicated in (5.12).

6. Numerical experiments. This section reports on four numerical experiments to study the accuracy of the introduced error estimators and the performance of the proposed adaptive strategy. All experiments have been conducted using MATLAB. All examples are academic in the sense that the exact solution is always known and we can compare the convergence of the error $E_h = |\!|\!| u - u_h |\!|\!|$ with the convergence of the error estimators. All experiments were performed with the parameter $\ell = 2, 3, 4$ in Algorithm 5.1. Since the numerical outcome looks similar, we restrict the presentation to the simplest case $\ell = 2$. The right-hand side for the Galerkin method is always computed as explained in section 5.4.

The first two examples are related to Neumann problems; cf. section 5.1. The solution for the example in section 6.1 is smooth and satisfies the regularity assumptions of section 4 so that the higher-order term in the error estimates satisfies $|\!|\!| u - \mathbb{G}_H u |\!|\!| = \mathcal{O}(h^{5/2})$. The solution for the example in section 6.2 corresponds to a classical finite element test problem on the (rotated) L-shaped domain which lacks H^2-regularity. For the generic corner singularity $U(r,\varphi) = r^\alpha \cos(\alpha\varphi)$ with $\alpha = 2/3$ for the reentrant corner $3\pi/2$, the corresponding Neumann data are (piecewise) smooth. In the example in section 6.3, we therefore consider the same example with $\alpha = 3/7$. Then, the Neumann data are singular at the reentrant corner and uniform mesh-refinement leads to a suboptimal convergence rate for the numerical solution of the hypersingular integral equation. This can be overcome by use of adaptive mesh-refinement. Finally, the example in section 6.4 considers a slit problem on the slit $\Gamma = [-1,1] \times \{0\}$. The right-hand side simplifies since the adjoint double layer potential vanishes; i.e., we do not have to deal with further quadrature errors to compute the right-hand side. The exact solution lies in $\widetilde{H}^{1-\varepsilon}(\Gamma)$ for any $\varepsilon > 0$.

6.1. Neumann problem with smooth solution. We consider the Neumann problem (5.1) on the halved unit square $\Omega = [0, 1/2]^2$ with exact solution

$$U(x,y) = \sinh(2\pi\, x)\, \cos(2\pi\, y) \tag{6.1}$$

and solve the corresponding hypersingular integral equation $Wu = f$ with right-hand side $f = (1 - K^*)g$ and $g = \partial U/\partial\nu$. Note that $\int_\Gamma U(x)\, ds_x = 0$. Therefore, the exact solution u of the hypersingular integral equation is just the trace on the boundary $u = U|_\Gamma$. The computation of the right-hand side for the Galerkin method is performed as shown in section 5.4 with the arclength derivative $u' = \nabla U(x) \cdot \tau(x)$ for the tangential vector $\tau(x)$ on Γ. Figure 1 shows initial mesh and the corresponding discrete solution u_h (for $\ell = 2$ in Algorithm 5.1) as a function of the arclength parameter $0 \le s \le 2$, where $s = 0$ corresponds to the point $(0,0)$ and counter-clockwise parametrization of the boundary $\Gamma = \partial\Omega$. The exact solution u is shown for comparison. Figure 2 shows the error

$$E_h := |\!|\!| u - u_h |\!|\!| = (|\!|\!| u |\!|\!|^2 - |\!|\!| u_h |\!|\!|^2)^{1/2},$$

where $|\!|\!| u |\!|\!| = 258.4278864$ (obtained from Aitkin's Δ^2 extrapolation of the sequence on uniformly refined meshes) as well as the introduced error estimators for uniform mesh-refinement. The values are plotted over the number $n^{(k)}$ of elements in the

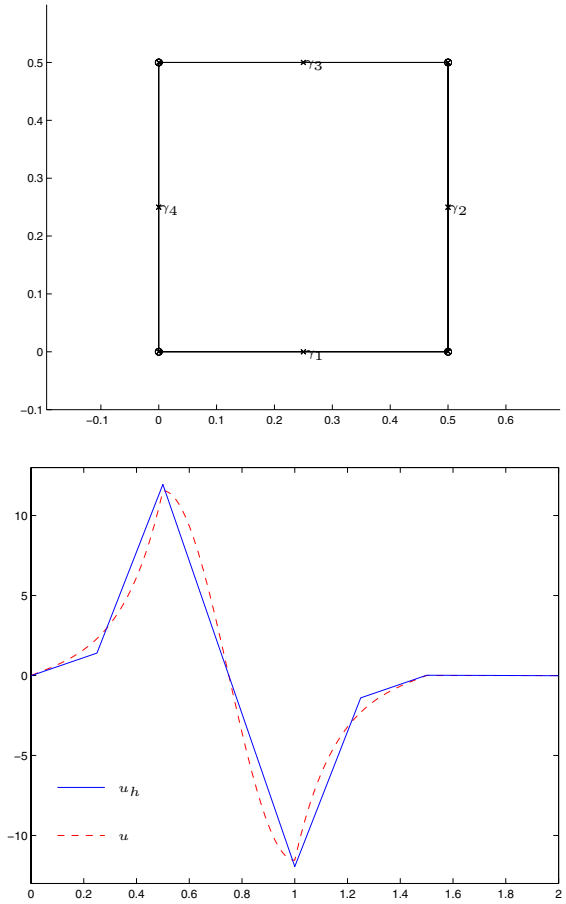

FIG. 1. *Initial coarse mesh* $\mathcal{T}_H^{(0)}$ *in the Neumann problem in section* 6.1 *with* $N = 4$ *elements (nodes indicated by* o*) (top) and the corresponding fine mesh* $\mathcal{T}_h^{(0)}$ *for* $\ell = 2$ *in Algorithm* 5.1*; i.e.,* $n = 8$ *(nodes indicated by* x*). The related discrete solution* u_h *on* $\mathcal{T}_h^{(0)}$ *(bottom) is plotted over the arclength* $s = 0, \dots, 2$ *of* Γ*. The exact solution* u *(i.e., the trace of* U *from* (6.1)*) is shown for comparison (bottom).*

kth fine grid $\mathcal{T}_h^{(k)}$. As is to be expected, uniform mesh-refinement leads to optimal experimental convergence rate

$$\kappa^{(k)}(E_h) := \log(E_h^{(k-1)}/E_h^{(k)}) \,/\, \log(n^{(k)}/n^{(k-1)}). \tag{6.2}$$

Here, $E_h^{(j)}$ denotes the error corresponding to the jth mesh (i.e., on the fine mesh in the jth step of Algorithm 5.1) with $n^{(j)}$ elements. The experimental convergence rate is visualized in Figure 2 through the slope of the interpolated values plotted in double-logarithmic scale. From the regularity of the exact solution $u = U|_\Gamma$ one expects convergence rate 3/2 for the error E_h and 5/2 for the error $E_H := \|\!|u - \mathbb{G}_H u|\!\|$ in a Galerkin scheme with $\mathcal{S}_0^2$ ansatz functions (cf. section 3.2), and this is in fact observed in Figure 2. Note that the assumptions of Theorem 4.2 are satisfied and η_M is an upper bound for the error E_h up to terms of higher order $\mathcal{O}(h^{5/2})$. We

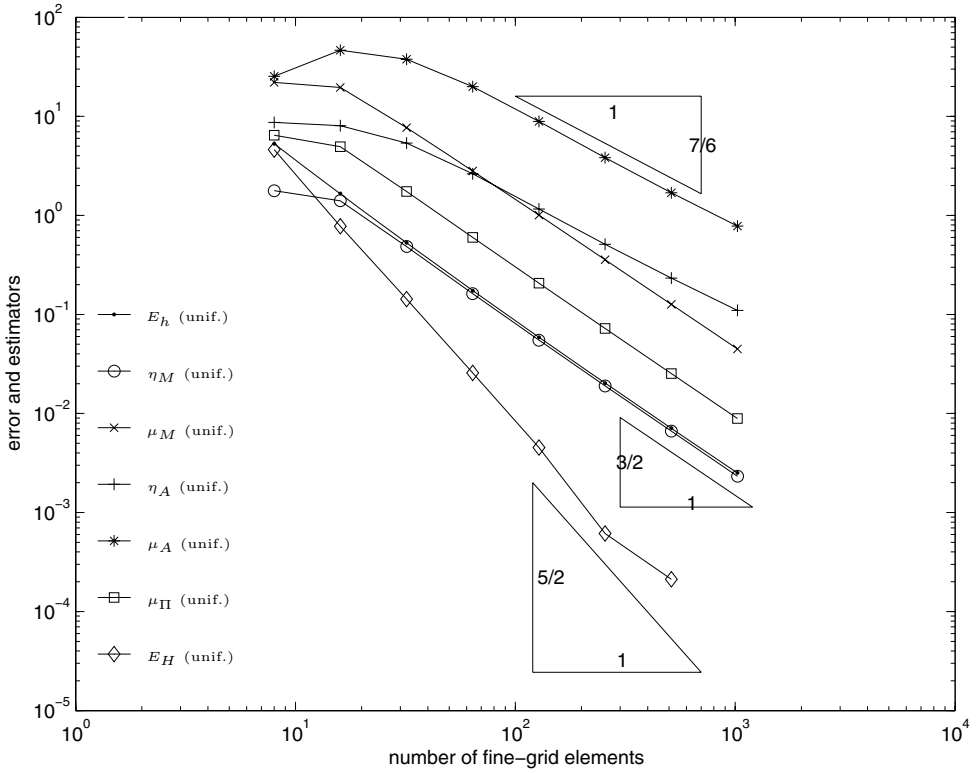

FIG. 2. *Error $E_h = \|(\mathbb{1} - \mathbb{G}_h)u\|$ and error estimators η_M, μ_M, η_A, μ_A, and μ_Π for $\ell = 2$ and uniform mesh-refinement in the Neumann problem in section* 6.1. *For comparison, we further show the S_H-error $E_H = \|(\mathbb{1} - \mathbb{G}_H)u\|$ which is of higher order: As expected from section* 3.2, *we observe $\kappa(E_h) = 3/2$ and $\kappa(E_H) = 5/2$. The estimators η_A and μ_A lack the efficiency, showing an experimental convergence rate less than* 3/2. *On the other hand, we observe reliability of μ_Π. Note that η_M is a very accurate estimator for E_h in the sense that both curves almost coincide.*

see that η_M is a very accurate estimate for E_h: The curves for E_h and η_M almost coincide. (See also Table 1, where we provide some numbers for $\ell = 1, \dots, 8$.) The error estimator μ_M is expected and observed to be reliable (for uniformly refined meshes) and efficient: The curve of μ_M is parallel to that of E_h and η_M. The same holds for the error estimator μ_Π which was only proved to be efficient in Corollary 4.5. The error estimators μ_A and η_A show reliability but obviously lack the efficiency: The curves for μ_A and η_A are parallel (as expected from Proposition 4.6) with slope 7/6. The failing efficiency estimate probably results from the lack of H^1 stability of the L^2 projection $\mathcal{A}_H : H^1(\Gamma) \to \mathcal{S}^2_0(\mathcal{T}) \subseteq H^1(\Gamma)$.

Figure 3 visualizes the error E_h and the error estimator μ_Π for uniform and adaptive mesh-refinement. As for uniform mesh-refinement, we obtain the experimental reliability of μ_Π: The curve of E_h and the corresponding curve of μ_Π are always parallel. Even for μ_A-adaptive mesh-refinement, where the error curve shows some zigzag behavior, this is imitated by the curve of μ_Π. All mesh-refining strategies recover the optimal convergence rate $\kappa(E_h) = 3/2$. Although adaptive mesh-refinement is not necessary for this example, the absolute values of E_h recommend the use of μ_M- or μ_Π-adaptive mesh-refinement. This is caused by the vanishing solution $u(x, y)$ for

TABLE 1

Index $\varrho = \|u-u_h\|/\eta_M$ for the Neumann problem in section 6.1 *with respect to the number $|\mathcal{T}_H|$ of coarse grid elements and the refinement parameter ℓ in Algorithm* 5.1. *One expects that ϱ tends to* 1 *for $\#\mathcal{T}_H, \ell \to \infty$ (cf. Theorem* 4.2*): In this case, the higher-order term $\|u - \mathbb{G}_H u\|$ tends to zero, and the constant $1/(1-L)$ tends to* 1. *Note that we used Aitkin's extrapolation rowwise to compute $\|u\|$ since the extrapolated value is affected by the quadrature errors to compute the right-hand side; cf. section* 5.4.

	$\ell = |\mathcal{T}_h|/|\mathcal{T}_H|$						
$|\mathcal{T}_H|$	2	3	4	5	6	7	8
4	2.98e+00	6.54e-01	3.75e-01	2.53e-01	1.85e-01	1.43e-01	1.15e-01
8	1.18e+00	8.49e-01	6.06e-01	4.46e-01	3.41e-01	2.70e-01	2.20e-01
16	1.09e+00	9.50e-01	8.08e-01	6.70e-01	5.52e-01	4.58e-01	3.84e-01
32	1.07e+00	9.96e-01	9.37e-01	8.65e-01	7.84e-01	7.02e-01	6.24e-01
64	1.07e+00	1.01e+00	9.87e-01	9.60e-01	9.28e-01	8.88e-01	8.43e-01
128	1.07e+00	1.02e+00	1.00e+00	9.91e-01	9.91e-01	9.68e-01	9.51e-01
256	1.07e+00	1.02e+00	1.00e+00	9.85e-01	1.04e+00	1.09e+00	9.91e-01
512	1.06e+00	1.03e+00	1.00e+00	9.70e-01	1.09e+00	1.20e+00	1.00e+00

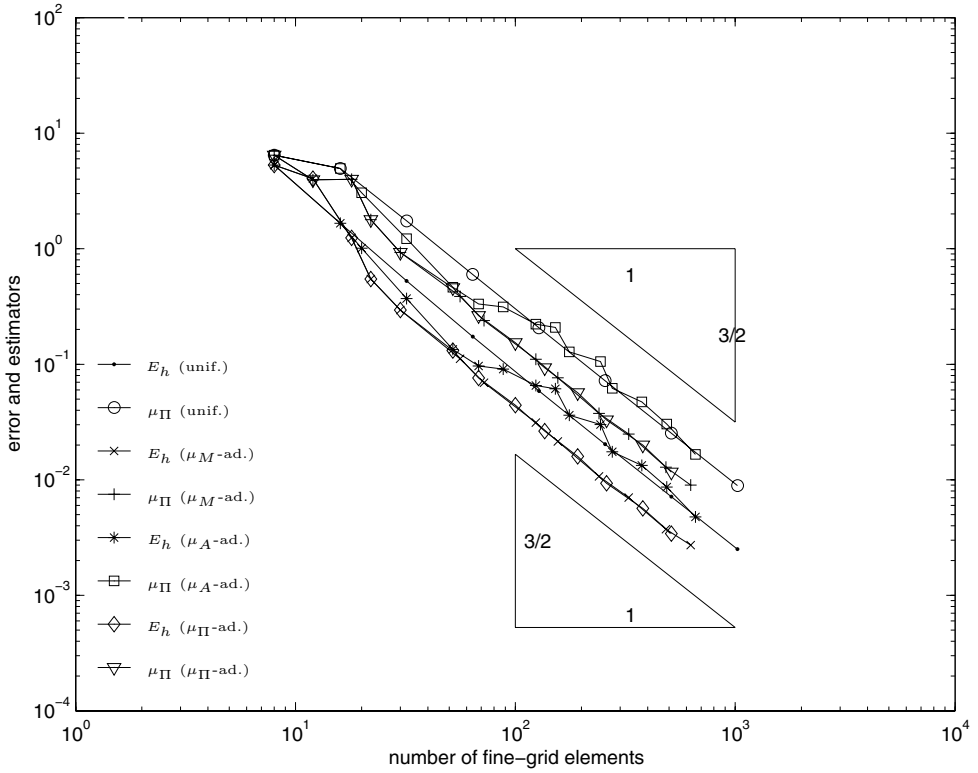

FIG. 3. *Error $E_h = \|(\mathbf{1} - \mathbb{G}_h)u\|$ and error estimator μ_Π in the example in section* 6.1 *for uniform (unif.) and adaptive (ad.) mesh-refinement and $\ell = 2$. Besides the efficiency of μ_Π proven in Corollary* 4.5 *one observes reliability of μ_Π: In all cases, the curves of E_h and μ_Π are parallel—even for μ_A-adaptive mesh-refinement.*

$x = 0$. We do not need any boundary elements there. The μ_A-adaptive mesh-refinement leads to absolute values of E_h which are even worse than the uniform mesh-refinement.

Some adaptively generated meshes are shown in Figure 4. For μ_M- and μ_Π-adaptive mesh-refinement, we see a strong refinement around the arclength parameter $s = 1/2$ and $s = 1$, where the exact solution has strong gradients; cf. Figure 1.

Finally, Figure 5 provides a comparison of the different estimators in dependence on the mesh-refining strategy. To make the subplots comparable we always print the outcome for uniform mesh-refinement. For all mesh-refining strategies, we see that η_A and μ_A are equivalent and reliable but lack the efficiency. The convergence rates for η_A and μ_A for adaptive mesh-refinement become even worse than for uniform mesh-refinement. On the other hand, we prove experimentally the reliability of μ_M (and μ_Π) even for non–quasi-uniform meshes.

6.2. Neumann problem with slightly singular solution. For a fixed parameter $\alpha > 0$, we consider the Neumann problem (5.1) on the L-shaped domain Ω shown in Figure 6 with exact solution

$$U(x) = \mathrm{Re}(x^\alpha) = r^\alpha \cos(\alpha\varphi) \quad \text{in polar coordinates} \quad x = r\,(\cos\varphi, \sin\varphi). \tag{6.3}$$

With the Dirichlet data $U|_\Gamma$, the exact solution u of (1.1) in $H^1_0(\partial\Omega)$ is given by $u = U|_\Gamma - \langle U|_\Gamma\,, 1\rangle/\langle 1\,, 1\rangle$. Numerical quadrature yields $\langle U|_\Gamma\,, 1\rangle/\langle 1\,, 1\rangle = 0.2095275$. The exact solution u is plotted over the arclength in Figure 6 for comparison with the discrete Galerkin solution. As in the previous section, the right-hand side in the Galerkin scheme is computed by use of the exact solution; cf. section 5.4. The gradient of $U(x)$ reads in polar coordinates as

$$\nabla U(x) = \alpha r^{\alpha-1} \begin{pmatrix} \cos(\varphi)\cos(\alpha\varphi) + \sin(\varphi)\sin(\alpha\varphi) \\ \sin(\varphi)\cos(\alpha\varphi) - \cos(\varphi)\sin(\alpha\varphi) \end{pmatrix}. \tag{6.4}$$

For the numerical experiment we choose $\alpha = 2/3$, which corresponds to the typical corner singularity at a reentrant corner with angle $3\pi/2$. The Neumann problem then leads to $U \notin H^2(\Omega)$. Nevertheless, the Dirichlet data are smooth as can be seen in Figure 6. Thus, we observe optimal experimental convergence rate $3/2$ [in terms of number of elements] even for uniform mesh-refinement. Figure 7 visualizes the error E_h and the error estimators η_M and μ_Π for uniform and adaptive mesh-refinement. As in the example in section 6.1, we observe that both error estimators are reliable and efficient. μ_M- and μ_Π-adaptive mesh-refinement lead to optimal experimental convergence rate $\kappa(E_h) = 3/2$ and even the absolute values of E_h are superior to the values obtained from uniform mesh-refinement. The μ_A-adaptive mesh-refinement leads to a curve with absolute values E_h even worse than for uniform mesh-refinement.

Some adaptively generated meshes are shown in Figure 8 for comparison. The meshes generated by μ_M-related and μ_Π-related mesh-refinement are very similar. This can also be observed from the plot in Figure 7, where the curves corresponding to μ_M and μ_Π, respectively, almost coincide.

Independent of the mesh-refining strategy, the estimator η_M provides an accurate estimate for the error E_h: The curves for E_h and η_M, which are related to the same mesh-refinement, coincide.

6.3. Problem with singular solution. We consider the same example as in section 6.2 but now with $\alpha = 3/7$, which leads to a singular exact solution u. Figure 9 shows the discrete solution u_h on the initial mesh $\mathcal{T}_h^{(0)}$ and, for comparison, the Dirichlet data $U|_\Gamma$ (up to an additive constant). Note that we subtracted the constant $\langle U|_\Gamma\,, 1\rangle/\langle 1\,, 1\rangle = 0.4205278$ from the Dirichlet data to obtain the unique solution u

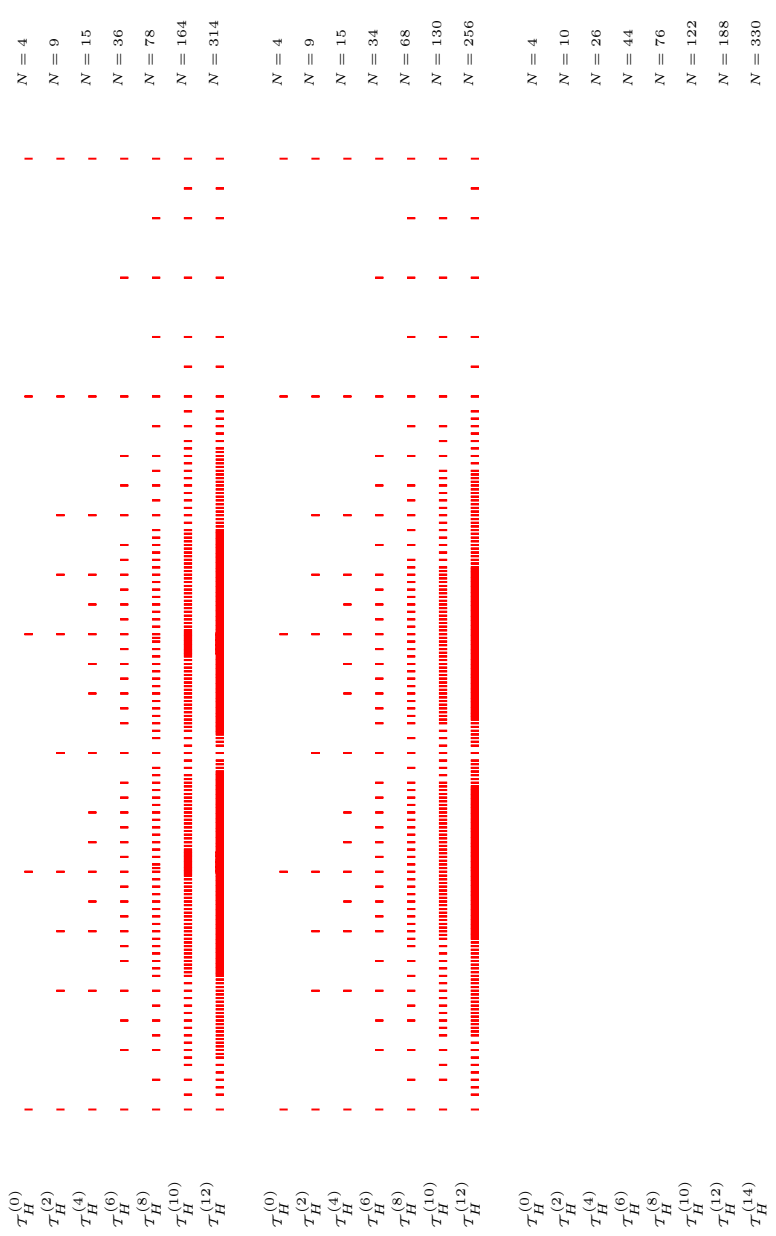

FIG. 4. *Adaptive mesh-refinement in the Poisson problem in section* 6.1 *with* $\ell = 2$ *related to the error estimator* μ_M *(top),* μ_Π *(middle), and* μ_A *(bottom), respectively.*

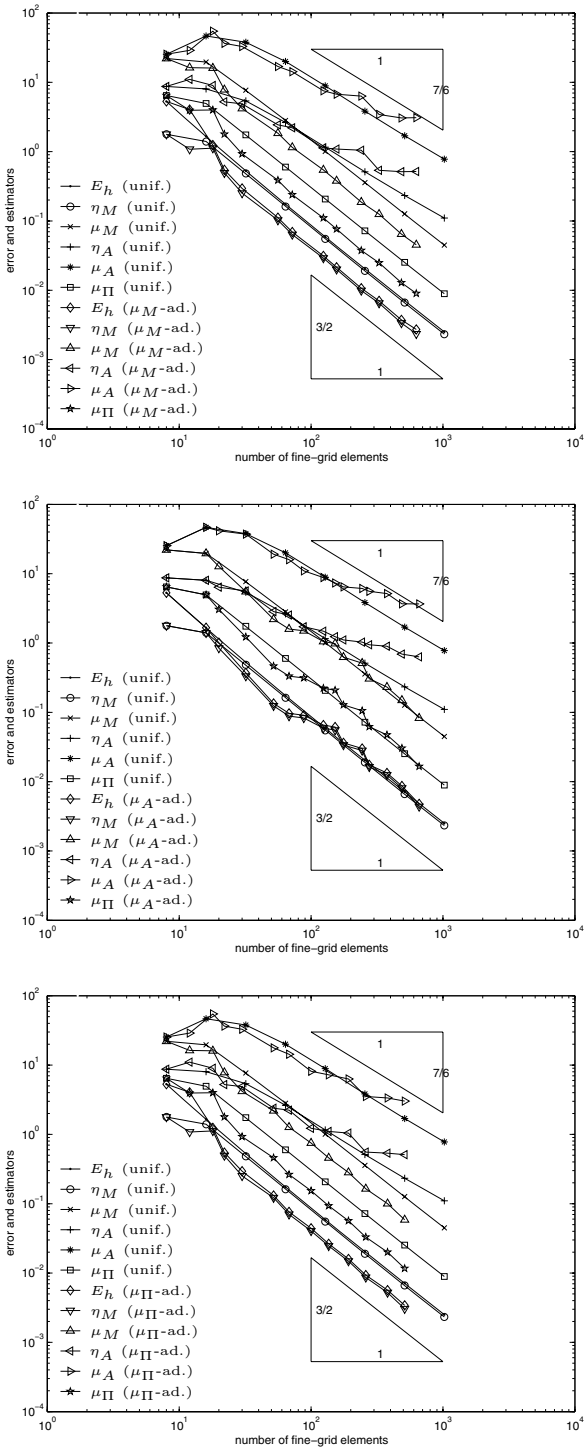

FIG. 5. *Error* $E_h = \|(\mathbf{1} - \mathbb{G}_h)u\|$ *and error estimator* μ_Π *in the example in section* 6.1 *for* $\ell = 2$ *and uniform (unif.) (resp., different adaptive (ad.)) mesh-refining strategies. In any case, we observe that the error estimators* η_M, μ_M, *and* μ_Π *are reliable and efficient. All mesh-refining strategies lead to optimal convergence rate* $\kappa(E_h) = 3/2$, *and* η_M *and* E_h *almost coincide. The error estimators* η_A *and* μ_A *lack the efficiency.*

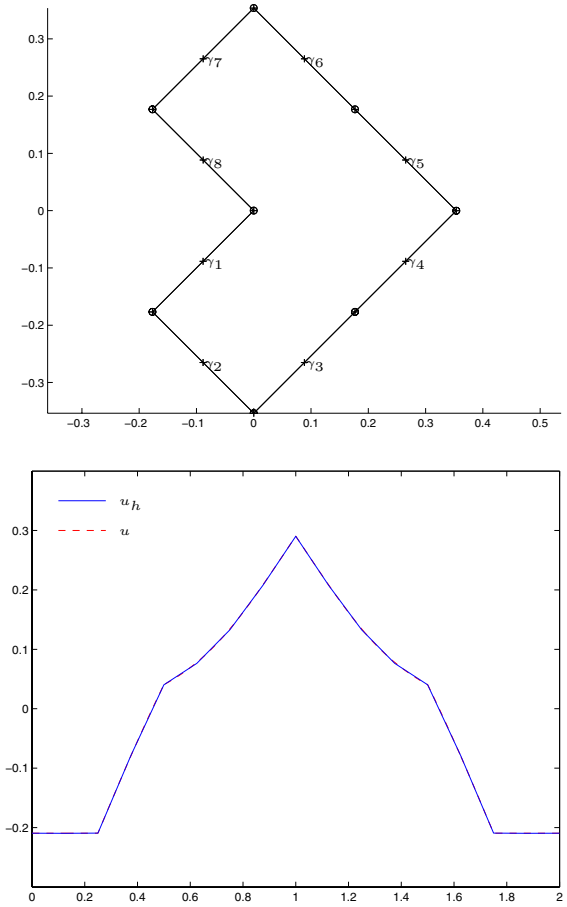

FIG. 6. *Initial coarse mesh* $\mathcal{T}_H^{(0)}$ *in the example in section* 6.2 *with* $N = 8$ *elements (nodes indicated by* ∘*) (top) and the corresponding fine mesh* $\mathcal{T}_h^{(0)}$ *for* $\ell = 2$ *in Algorithm* 5.1*, i.e.,* $n = 16$ *(nodes indicated by* +*). The related discrete solution* u_h *on* $\mathcal{T}_h^{(0)}$ *(bottom) is plotted over the arclength* $s = 0, \dots, 2$ *of* Γ*. The exact solution* u *is shown for comparison (bottom). Note that, due to the resolution of the bottom figure, there is almost no visible difference between* u *and* u_h*.*

of (1.1) in $H_0^1(\partial\Omega)$. As can be seen, the exact solution now yields a singularity at the reentrant corner at arclength $s = 0$ and $s = 2$, respectively.

Uniform mesh-refinement leads to a suboptimal experimental convergence rate of 3/7 for the error E_h. Figure 10 visualizes the error E_h as well as the error estimators η_M and μ_Π for uniform, and μ_M-, μ_A-, and μ_Π-adaptive, mesh-refinement. The μ_M- and μ_A-adaptive strategies recover the optimal convergence rate 3/2, which is experimentally obtained from the very start; i.e., there is no preasymptotic behavior as is normally observed for adaptive methods. The adaptively generated meshes, visualized in Figure 11, look very similar for both strategies, and the related E_h-curves coincide. This is very different for the μ_A-adaptive mesh-refinement. After a small preasymptotic phase (for $n \leq 40$) and compared with the uniform mesh-refinement, we observe an improvement of the experimental convergence rate. However, the μ_A-adaptive strategy does not seem to recover the optimal convergence rate. The μ_A-adaptively

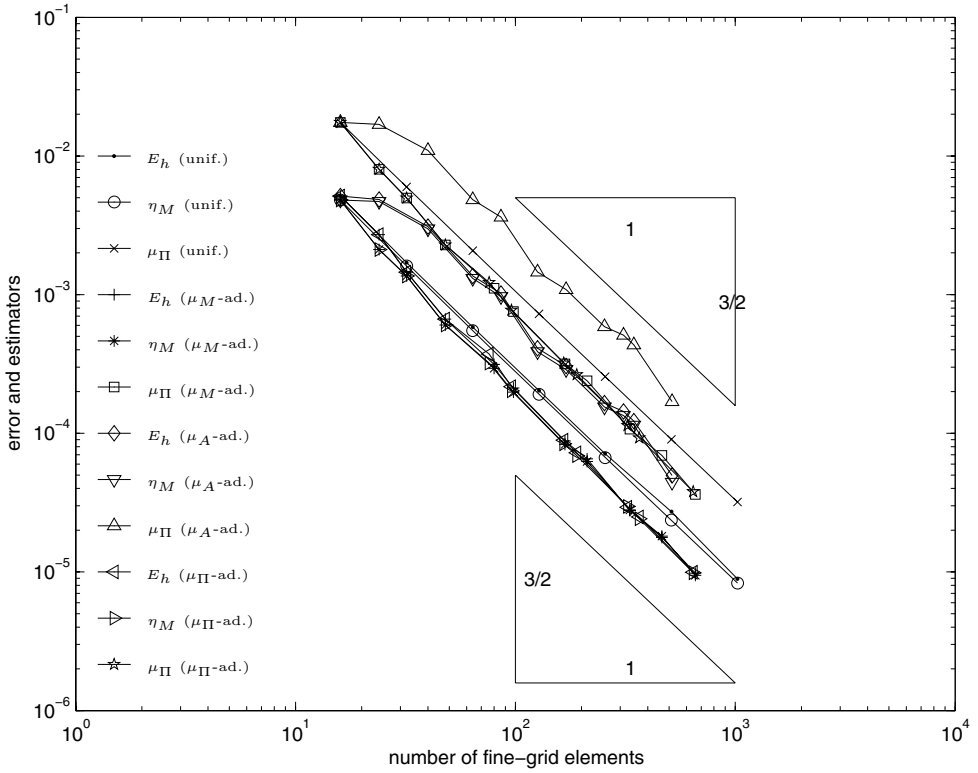

FIG. 7. *Error* $E_h = \|(\mathbf{1} - \mathbb{G}_h)u\|$ *and error estimator* μ_Π *in the example in section* 6.2 *for uniform (unif.) and adaptive (ad.) mesh-refinement and* $\ell = 2$. *Besides the efficiency of* μ_Π *proven in Corollary* 4.5 *one observes reliability of* μ_Π. *The error estimator* η_M *estimates* E_h *very accurately: The values almost coincide independent of the mesh-refining strategy. Whereas* μ_M*- and* μ_Π*-adaptive mesh-refinement lead to improved absolute values for the error* E_h, *the* E_h*-curve for* μ_A*-adaptive mesh-refinement is above the curve corresponding to uniform mesh-refinement; i.e., the absolute value of* E_h *for a fixed number of unknowns is even worse than for uniform mesh-refinement.*

generated meshes show some further mesh-refinement where the exact solution u has some local maxima (cf. Figures 9 and 11), which is not necessary when compared with the optimal results for μ_M- and μ_Π-adaptive mesh-refinement.

The error estimation by η_M is not as good as that observed in the preceding examples. This is probably due to the fact that the term $\|u - \mathbb{G}_H u\|$ now is *not* a higher-order term.

6.4. Slit problem with exact solution. Our last example is concerned with the hypersingular integral equation (1.1) with constant right-hand side $f \equiv 1$ on the slit $\Gamma = [-1, 1] \times \{0\}$. The exact solution u is given by

$$u(x, 0) = \sqrt{1 - x^2} \quad \text{for } (x, 0) \in \Gamma. \tag{6.5}$$

There holds $u \in \widetilde{H}^{1-\varepsilon}(\Gamma)$ for all $\varepsilon > 0$, but $u \notin \widetilde{H}^1(\Gamma)$. The energy norm of u can be computed analytically, $\|u\| = \sqrt{\pi/2}$. Figure 12 shows the experimental results of our computations. As in the previous examples, the error estimators η_M, μ_M, and μ_Π show

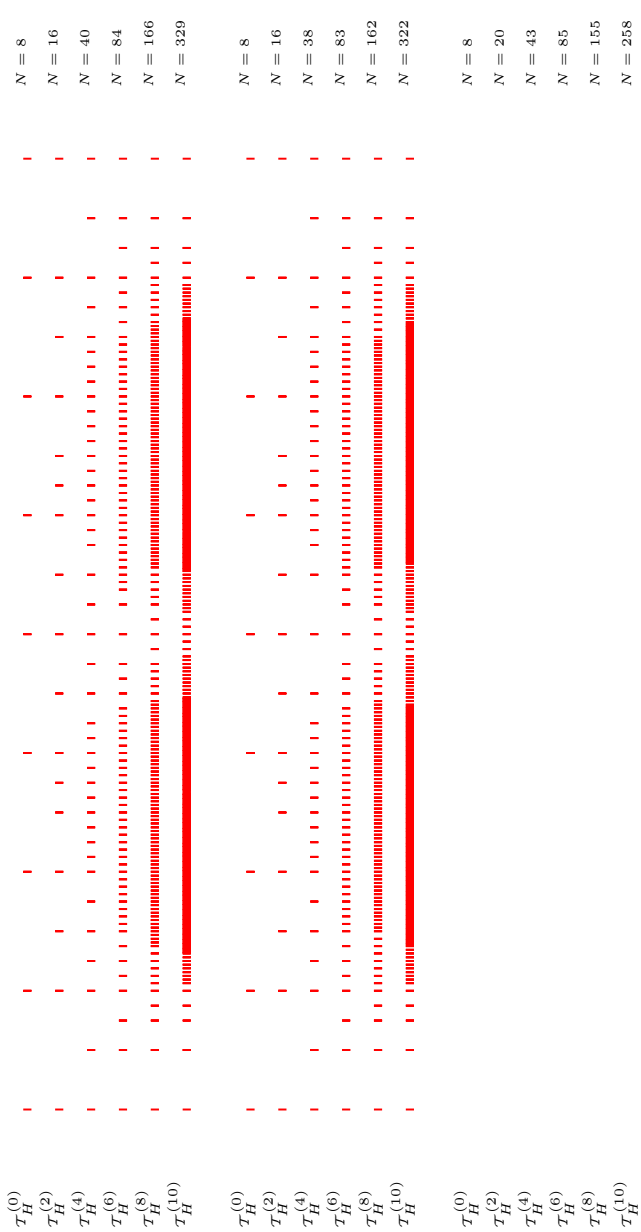

FIG. 8. *Adaptive mesh-refinement in the Poisson problem in section* 6.2 *with* $\ell = 2$ *related to the error estimator* μ_M *(top),* μ_Π *(middle), and* μ_A *(bottom), respectively. For the* μ_M*- and* μ_Π*-adapted meshes, we see a high mesh-refinement towards the reentrant corner, where* u *is slightly singular.*

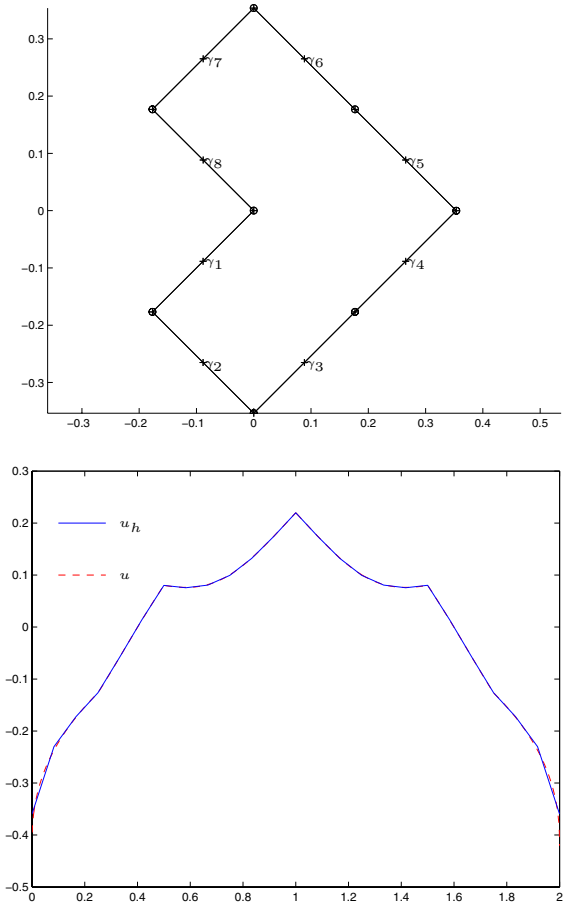

FIG. 9. *Initial coarse mesh* $\mathcal{T}_H^{(0)}$ *in the example in section* 6.3 *with* $N = 8$ *elements (nodes indicated by* ∘*) (top) and the corresponding fine mesh* $\mathcal{T}_h^{(0)}$ *for* $\ell = 2$ *in Algorithm* 5.1. *The related discrete solution* u_h *on* $\mathcal{T}_h^{(0)}$ *as well as the exact solution* u *is plotted over the arclength* $s = 0, \dots, 2$ *of* Γ *(bottom).*

efficiency and reliability independent of the mesh-refining strategy. Uniform mesh-refinement leads to a suboptimal experimental convergence rate $\kappa(E_h) = \mathcal{O}(h^{1/2})$. This can be improved by use of μ_M- and μ_Π-adaptive mesh-refinement. Both adaptive strategies recover the optimal convergence rate. As in the example in section 6.3, μ_A-adaptive mesh-refinement leads to an improved convergence rate of the error, but this is still suboptimal.

7. Conclusions.

7.1. Empirical results. The overall impressions of our numerical experiments, partly repeated from the preceding subsections, give us the subsequent empirical results.

(a) μ_Π is the most simple estimator (from the conceptual and implementational point of view); it is theoretically shown only to be efficient, but performs efficiently and reliably in our numerical examples.

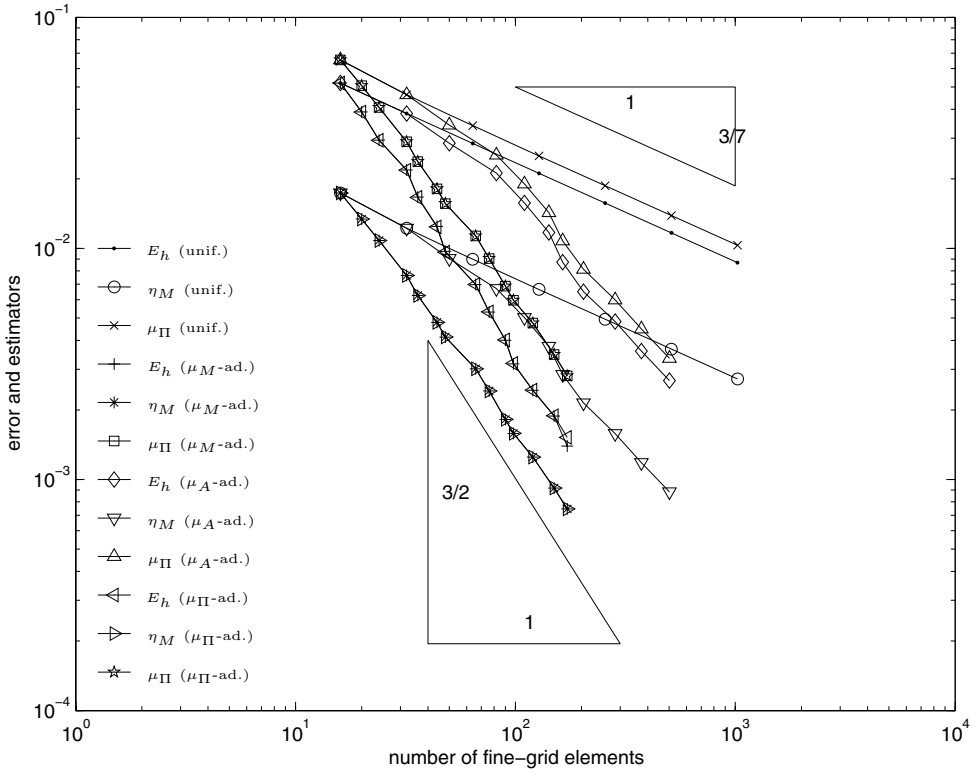

FIG. 10. *Error* $E_h = \|(\mathbb{1} - \mathbb{G}_h)u\|$ *and error estimators* η_M, μ_M, *and* μ_Π *for uniform (unif.),* μ_M*-adaptive (*μ_M*-ad.), and* μ_Π*-adaptive (*μ_Π*-ad.) mesh-refinement in the example in section* 6.3 *with* $\ell = 2$ *in Algorithm* 5.1.

(b) The error control of η_M is extremely accurate at least if the exact solution u has some regularity. The error estimation is far superior in comparison with the other error estimators.

(c) Algorithm 5.1 steered by the refinement indicators μ_M and μ_Π, respectively, leads to the optimal experimental convergence rate of the Galerkin method whenever the regularity of the exact solution leads to a reduced convergence order for uniform mesh-refinement.

(d) For $\mathcal{A}_H$, the L^2 projection onto $\mathcal{S}_H$, the error estimators η_A and μ_A lack the efficiency. Although μ_A-adaptive mesh-refinement leads to an improvement of the experimental convergence rate for the singular examples, this adaptive strategy does not regain the optimal convergence rate.

(e) The numerical outcome appears to be very sensitive with respect to implementational details. The estimators η_M, μ_M, and η_A involve stiffness matrices with respect to $\mathcal{S}_0^2$, while μ_Π relies on the much more robust L^2 projection.

7.2. Theoretical results. The heart of our analysis is Proposition 4.1 and, obtained from this, the efficiency and reliability of the error estimator $\eta_M = \|u_h - \mathbb{G}_H u_h\|$ up to terms of higher order. Those higher-order terms depend only on the regularity of the exact solution u which is in general unknown.

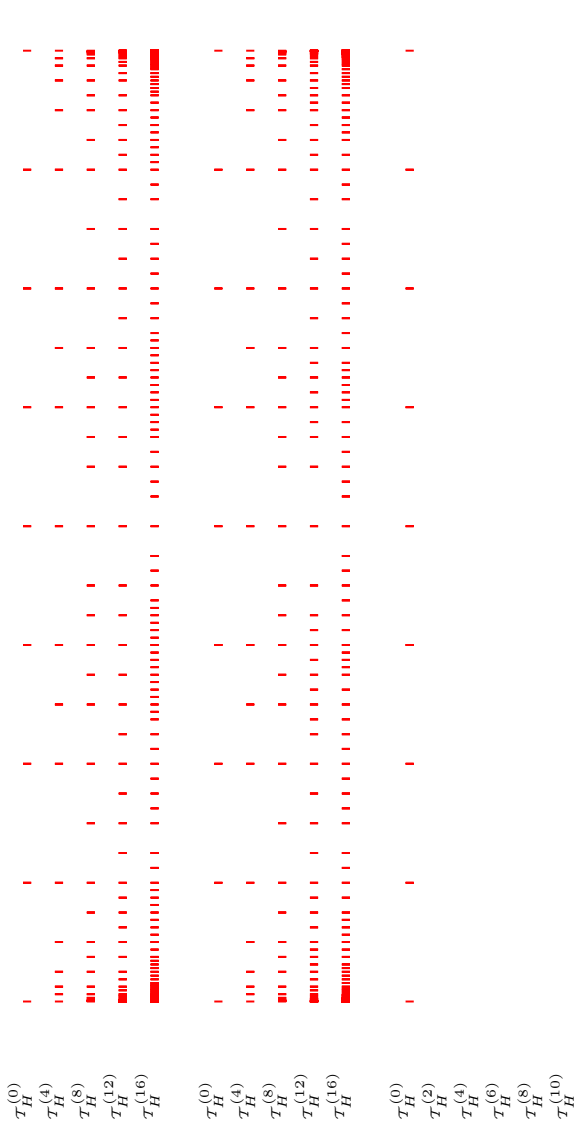

FIG. 11. *Adaptive mesh-refinement in the Poisson problem in section* 6.3 *with* $\ell = 2$ *related to the error estimator* μ_M *(top),* μ_Π *(middle), and* μ_A *(bottom), respectively.*

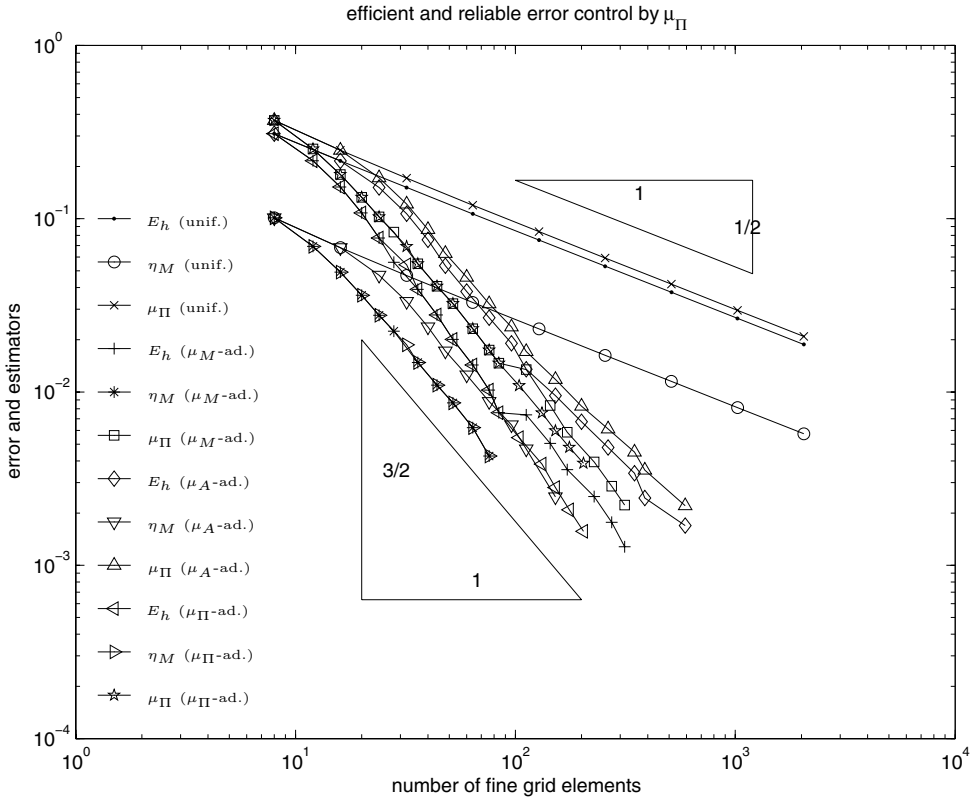

FIG. 12. *Error* $E_h = \|(\mathbf{1} - \mathbb{G}_h)u\|$ *and error estimators* η_M *and* μ_Π *for uniform (unif.) and adaptive (ad.) mesh-refinement in the example in section* 6.4 *with* $\ell = 2$ *in Algorithm* 5.1.

The proof of Proposition 4.1 has essentially two ingredients: first, an approximation operator $I_h : \mathcal{S}_H \to \mathcal{S}_h$ which has a local first-order approximation property, and second, a local inverse estimate in $\mathcal{S}_H$. Whereas we provided the inverse estimate for two- and three-dimensional problems, we did not provide the operator I_h in the latter case. For two dimensions, one can simply choose $I_h v_H$ to be the nodal interpolant. For three dimensions, one choice is (a slightly modified) Clément interpolation operator [FFP].

From the best approximation property of the Galerkin projection, one obtains that each averaging operator $\mathcal{A}_H : \mathcal{S}_h \to \mathcal{S}_H$ yields a reliable error estimator $\eta_A = \|u_h - \mathcal{A}_H u_h\|$.

Since the energy norm $\|\cdot\|$ is nonlocal, the obtained estimators cannot be employed for an adaptive mesh-refinement directly. We use localization in terms of the weighted H^1 seminorm $\mu_A = \|H^{1/2}(u_h - \mathcal{A}_H u_h)'\|_{L^2(\Gamma)}$. An inverse estimate shows the lower bound $C^{-1}\mu_A \le \eta_A$. The verification of $\eta_A \le C\,\mu_A$ needs some approximation property of $\mathcal{A}_H$ and holds, e.g., for the Galerkin projection $\mathcal{A}_H = \mathbb{G}_H$.

7.3. Future development. There remain several open questions for future research.

(a) From a comparison with the finite element method, the most natural error estimator is $\mu_\Pi = \|H^{1/2}(u_h' - \Pi_H u_h')\|_{L^2(\Gamma)}$ with Π_H the L^2 projection onto $\mathcal{P}^1(\mathcal{T}_H)$.

The proof of the reliability seems to need a different analytical technique, which is far beyond the scope of this paper.

(b) As for Symm's integral equation [CP], an analytical justification of Algorithm 5.1 would be desirable. The analytical verification of the introduced error estimators needs high regularity assumptions on u which are in general not satisfied and—according to our experiments—not necessary in praxis.

(c) The justification of η_M for the higher-order term $\|(\mathbb{1} - \mathbb{G}_H)u\|$ reads more precisely as follows, where $L < 1$ denotes the constant from (4.1): Provided that

$$\frac{1}{1-L}\,\frac{\|u - \mathbb{G}_H u\|}{\|u - u_h\|} =: \varrho_{hH} < 1, \tag{7.1}$$

Theorem 4.2 states that $\|u - u_h\| \le \frac{1}{1-L}\,\eta_M + \varrho_{hH}\|u - u_h\|$ and thus

$$\|u - u_h\| \le \frac{1}{(1-L)(1-\varrho_{hH})}\,\eta_M. \tag{7.2}$$

Sufficient smoothness of u (cf. (4.2)) justifies (7.1) for sufficiently small mesh-sizes h and H. However, singularities yield much poorer smoothness, e.g., $u \in H^s(\mathcal{T}_H)$ for $s \le \frac{3}{2} - \varepsilon$. Then, uniform meshes result in

$$\|u - u_h\| = C_7 h^\alpha + o(h^\alpha) \quad \text{and} \quad \|u - \mathbb{G}_H u\| = C_8 H^\alpha + o(H^\alpha)$$

for the same order of convergence $\alpha > 0$ as $h \to 0$. Then, there is no guarantee that

$$\varrho_{hH} = \frac{(H/h)^\alpha}{1-L}\,\frac{C_8}{C_7} + o(1)$$

satisfies $\varrho_{hH} < I$. However, because higher-order discrete spaces are better, one may expect that $C_8 < C_7$ so that there is room for (7.1). Since details depend on all the constants, a further analysis lies beyond the scope of this work.

(d) Three-dimensional experiments for Symm's integral equation and the hypersingular integral equation are postponed to a forthcoming paper [FFP].

Acknowledgment. Parts of this work were done when the second author (DP) enjoyed the hospitality of the Humboldt-Universität zu Berlin.

REFERENCES

[AC] J. Alberty and C. Carstensen, *Averaging techniques for reliable a posteriori FE-error control in elastoplasticity with hardening*, Comput. Methods Appl. Mech. Engrg., 192 (2003), pp. 1435–1450.

[BL] J. Bergh and J. Löfström, *Interpolation Spaces*, Grundlehren Math. Wiss. 223, Springer-Verlag, Berlin, 1976.

[C1] C. Carstensen, *An a posteriori error estimate for a first-kind integral equation*, Math. Comp., 66 (1997), pp. 69–84.

[C2] C. Carstensen, *Some remarks on the history and future of averaging techniques in a posteriori finite element analysis*, ZAMM Z. Angew. Math. Mech., 84 (2004), pp. 3–21.

[CB] C. Carstensen and S. Bartels, *Each averaging technique yields reliable a posteriori error control in FEM on unstructured grids.* I. *Low order conforming, nonconforming, and mixed FEM*, Math. Comp., 71 (2002), pp. 945–969.

[CFa] C. Carstensen and B. Faermann, *Mathematical foundation of a posteriori error estimates and adaptive mesh-refining algorithms for boundary integral equations of the first kind*, Eng. Anal. Bound. Elem., 25 (2001), pp. 497–509.

[CFuI] C. Carstensen and S. A. Funken, *Averaging technique for FE—A posteriori error control in elasticity.* I. *Conforming FEM*, Comput. Methods Appl. Mech. Engrg., 190 (2001), pp. 2483–2498.

[CFuII] C. Carstensen and S. A. Funken, *Averaging technique for FE—A posteriori error control in elasticity.* II. *λ-independent estimates*, Comput. Methods Appl. Mech. Engrg., 190 (2001), pp. 4663–4675.

[CFuIII] C. Carstensen and S. A. Funken, *Averaging technique for FE—A posteriori error control in elasticity.* III. *Locking-free nonconforming FEM*, Comput. Methods Appl. Mech. Engrg., 191 (2001), pp. 861–877.

[CP] C. Carstensen and D. Praetorius, *Averaging techniques for the effective numerical solution of Symm's integral equation of the first kind*, SIAM J. Sci. Comput., 27 (2006), pp. 1226–1260.

[CaS] C. Carstensen and E. P. Stephan, *Adaptive boundary element methods for some first kind integral equations*, SIAM J. Numer. Anal., 33 (1996), pp. 2166–2183.

[Co] M. Costabel, *Boundary integral operators on Lipschitz domains: Elementary results*, SIAM J. Math. Anal., 19 (1988), pp. 613–626.

[CoS] M. Costabel and E. P. Stephan, *The normal derivative of the double layer potential on polygons and Galerkin approximation*, Appl. Anal., 16 (1983), pp. 205–228.

[FFP] S. Funken, S. Ferraz-Leite, and D. Praetorius, *Averaging on Large Patches for First Kind Integral Equations in* 3*D*, work in progress, 2007.

[GHS] I. G. Graham, W. Hackbusch, and S. A. Sauter, *Finite elements on degenerate meshes: Inverse-type inequalities and applications*, IMA J. Numer. Anal., 25 (2005), pp. 379–407.

[HSWW] W. Hoffmann, A. H. Schatz, L. B. Wahlbin, and G. Wittum, *Asymptotically exact a posteriori estimators for the pointwise gradient error on each element in irregular meshes, Part* I*: A smooth problem and globally quasi-uniform meshes*, Math. Comp., 70 (2001), pp. 897–909.

[Ma] M. Maischak, *The Analytical Computation of the Galerkin Elements for the Laplace, Lamé and Helmholtz Equation in* 2*D-BEM*, preprint, Institut für Angewandte Mathematik, Universität Hannover, Hannover, Germany, 1999.

[McL] W. McLean, *Strongly elliptic systems and boundary integral equations*, Cambridge University Press, Cambridge, UK, 2000.

[SaS] S. A. Sauter and C. Schwab, *Randelemente, Analyse und Implementierung schneller Algorithmen*, Teubner, Stuttgart, Germany, 2004.

[ZZ] O. C. Zienkiewicz and J. Z. Zhu, *A simple error estimator and adaptive procedure for practical engineering analysis*, Internat. J. Numer. Methods Engrg., 24 (1987), pp. 337–357.